



## King's Research Portal

DOI:

[10.1038/s41591-018-0102-y](https://doi.org/10.1038/s41591-018-0102-y)

*Document Version*

Peer reviewed version

[Link to publication record in King's Research Portal](#)

*Citation for published version (APA):*

Sun, W., Dong, H., Becker, A. S., Dapito, D. H., Modica, S., Grandl, G., Opitz, L., Efthymiou, V., Straub, L. G., Sarker, G., Balaz, M., Balazova, L., Perdikari, A., Kiehlmann, E., Bacanovic, S., Zellweger, C., Peleg-Raibstein, D., Pelczar, P., Reik, W., ... Wolfrum, C. (2018). Cold-induced epigenetic programming of the sperm enhances brown adipose tissue activity in the offspring. *Nature Medicine*. <https://doi.org/10.1038/s41591-018-0102-y>

### **Citing this paper**

Please note that where the full-text provided on King's Research Portal is the Author Accepted Manuscript or Post-Print version this may differ from the final Published version. If citing, it is advised that you check and use the publisher's definitive version for pagination, volume/issue, and date of publication details. And where the final published version is provided on the Research Portal, if citing you are again advised to check the publisher's website for any subsequent corrections.

### **General rights**

Copyright and moral rights for the publications made accessible in the Research Portal are retained by the authors and/or other copyright owners and it is a condition of accessing publications that users recognize and abide by the legal requirements associated with these rights.

- Users may download and print one copy of any publication from the Research Portal for the purpose of private study or research.
- You may not further distribute the material or use it for any profit-making activity or commercial gain
- You may freely distribute the URL identifying the publication in the Research Portal

### **Take down policy**

If you believe that this document breaches copyright please contact [librarypure@kcl.ac.uk](mailto:librarypure@kcl.ac.uk) providing details, and we will remove access to the work immediately and investigate your claim.

1 **Cold-induced epigenetic programming of the sperm enhances brown**  
2 **adipose tissue activity in the offspring**

3  
4  
5  
6  
7  
8  
9 **Authors:**

10 Wenfei Sun<sup>1†</sup>, Hua Dong<sup>1†</sup>, Anton S. Becker<sup>1,3,4</sup>, Dianne Helerie Dapito<sup>1</sup>, , Salvatore  
11 Modica<sup>1</sup>, Gerald Grandl<sup>1</sup>, Lennart Opitz<sup>1,2</sup>, Vissarion Efthymiou<sup>1</sup>, Leon Gabriel Straub<sup>1</sup>,  
12 Gitalee Sarker<sup>1</sup>, Miroslav Balaz<sup>1</sup>, Lucia Balazova<sup>1</sup>, Aliko Perdikari<sup>1</sup>, Elke Kiehlmann<sup>1</sup>,  
13 Sara Bacanovic<sup>4</sup>, Caroline Zellweger<sup>4</sup>, Daria Peleg-Raibstein<sup>1</sup>, Pawel Pelczar<sup>5</sup>, Wolf  
14 Reik<sup>6,7</sup>, Irene A. Burger<sup>4</sup>, Ferdinand von Meyenn<sup>6,8</sup>, Christian Wolfrum<sup>1\*</sup>

15  
16  
17  
18  
19 **Affiliations:**

20 <sup>1</sup>Institute of Food, Nutrition and Health, ETH Zurich, Schwerzenbach, Switzerland

21 <sup>2</sup>Functional Genomics Center Zurich, ETH Zurich/University of Zurich, Zurich,  
22 Switzerland

23 <sup>3</sup>Institute of Diagnostic and Interventional Radiology, University Hospital of Zurich,  
24 Zurich, Switzerland

25 <sup>4</sup>Clinic of Nuclear Medicine, University Hospital of Zurich, Zurich, Switzerland

26 <sup>5</sup>Center for Transgenic Models, University of Basel, Basel, Switzerland

27 <sup>6</sup>Epigenetics Programme, Babraham Institute, Cambridge, United Kingdom

28 <sup>7</sup>Wellcome Trust Sanger Institute, Hinxton, United Kingdom.

29 <sup>8</sup>Department of Medical & Molecular Genetics, King's College London, London, UK

30  
31  
32  
33 \*Correspondence to:

34  
35 Swiss Federal Institute of Technology  
36 Department of Health Sciences and Technology  
37 CH-8603 Schwerzenbach  
38 christian-wolfrum@ethz.ch

39  
40 †These authors contributed equally to this work.

41

42 **Key Words**

43 Metabolic syndromes; Obesity; Brown adipose tissue; Transgenerational regulation

## 44 **Abstract**

45 Recent research has focused on environmental effects controlling tissue functionality  
46 and systemic metabolism. However, whether such stimuli affect human thermogenesis  
47 and body-mass index (BMI) has not been explored. Here, we show retrospectively that  
48 the presence of brown adipose tissue (BAT) and the season of conception are linked to  
49 BMI in humans. In mice, we demonstrate that cold exposure of males, but not females,  
50 before mating results in improved systemic metabolism and protection from diet induced  
51 obesity of the male offspring. Integrated analyses of the DNA methylome and RNA-seq  
52 of the sperm from male mice reveal several clusters of co-regulated differentially  
53 methylated regions (DMR) and differentially expressed genes (DEG), suggesting that  
54 the improved metabolic health of the offspring is due to enhanced BAT formation and  
55 increased neurogenesis. The conclusions are supported by cell-autonomous studies in  
56 the offspring demonstrating an enhanced capacity to form mature active brown  
57 adipocytes, improved neuronal density and more norepinephrine release in BAT in  
58 response to cold stimulation. Taken together, our results indicate that in humans and in  
59 mice seasonal or experimental cold exposure induces an epigenetic programming of the  
60 sperm such that the offspring harbor hyper-active BAT and an improved adaptation to  
61 overnutrition and hypothermia.

62

## 63 **Introduction**

64 In 2016, 39% of all adults worldwide were classified as overweight (BMI >25) and 13%  
65 as clinically obese (BMI >30) (ref. 1). This imposes a burden on society as obesity-  
66 associated co-morbidities, linked to an increase in adipose tissue mass, are the main  
67 contributors to overall mortality and health care costs. Adipose tissue functions as a

68 dynamic endocrine organ<sup>2</sup> and therefore its “quality” is considered to be an important  
69 factor in the development of obesity associated co-morbidities<sup>3</sup>. Adipose tissue can be  
70 divided into the functionally and morphologically distinct white (WAT) and brown adipose  
71 tissues (BAT)<sup>4</sup>. The main function of BAT is energy dissipation via non-shivering  
72 thermogenesis<sup>5</sup>, enabled by the presence of uncoupling protein 1 (UCP1) in the inner  
73 mitochondrial membrane. Thus, brown adipocytes contribute to the maintenance of body  
74 temperature during acute and chronic cold exposure<sup>2,6</sup>.

75 Besides classical BAT found in rodents in the interscapular area (iBAT), a second  
76 type of thermogenic active fat cell (termed beige or brite adipocytes) has been described  
77 which is induced by cold exposure mainly in inguinal WAT (ingWAT)<sup>7</sup>. Analysis of <sup>18</sup>F-  
78 Fluorodeoxyglucose (FDG)-PET/CT scans demonstrated the presence of active BAT in  
79 adult humans, in supraclavicular, paravertebral and deep neck regions<sup>8-13</sup> and human  
80 BAT can be activated by mild cold exposure or by administration of a specific adrenergic  
81 receptor beta 3 (ADRB3)-agonist<sup>14,15</sup>. The relevance of BAT for physiology was inferred  
82 by the association with various metabolic parameters<sup>15</sup> and it was demonstrated that  
83 people with functional BAT can effectively lose weight by a mild cold stimulation  
84 regime<sup>16</sup>.

85 In recent years, studies have demonstrated a link between paternal  
86 preconception nutrient exposure and the phenotype of the offspring<sup>17,18</sup>. Differences in  
87 gene expression patterns arise during development and can be retained through mitosis  
88 by epigenetic mechanisms<sup>19</sup>. In the context of thermoregulation, it was shown that  
89 environmentally-induced changes in gene expression can affect cellular function and  
90 thereby also the predisposition to certain diseases<sup>20</sup>. Additionally, changes in the  
91 environment can be transmitted to subsequent generations<sup>18,21,22</sup>. More specifically,

92 there have been indications that the season of birth and adult BMI show some  
93 correlation<sup>23</sup>. Here we studied the influence of environmental temperature and its effect  
94 on systemic metabolism, as well as the contribution of different thermogenic pathways  
95 using human and mouse studies.

96

### 97 **Cold exposure before conception and during gestation activates brown and white** 98 **adipose tissue**

99 To identify a possible correlation between ambient temperature and BAT abundance, we  
100 performed a retrospective study of FDG-PET/CT scans from 2007 – 2015 collected from  
101 the University Hospital of Zurich ( $n = 8440$  individuals). Representative PET images  
102 from two individuals are shown in **Supplementary Fig. 1a**. Individuals with active BAT  
103 were 3.2% more likely to have been conceived in the colder period of the year, e.g.  
104 between October and February (mean temperature estimate 2 °C), while individuals  
105 without active BAT were more likely conceived in the warmer months, e.g. between April  
106 and September (mean temperature estimate 13 °C) (**Fig. 1a**). No apparent fluctuations  
107 in age (**Supplementary Fig. 1b**) or BMI (**Supplementary Fig. 1c**) were observed and  
108 the pattern persisted for different BAT activation strengths (**Supplementary Fig. 1d**).  
109 Among individuals conceived in the colder period ( $n = 3793$ ), BAT positive individuals ( $n$   
110 = 235) had a significantly lower BMI (mean 20.9 vs. 22.8;  $p < 0.001$ ) compared to age-  
111 and sex-matched BAT-negative individuals (**Fig. 1b**). These data identify a correlation  
112 between the season of conception and the propensity to form active BAT; however,  
113 given the retrospective nature and the large number of potential confounders, causality  
114 cannot be inferred. Hence, we investigated the effect of cold exposure (CE) before and  
115 during conception using mouse model systems. We analyzed offspring groups whose

116 parents had not been exposed to cold (23 °C) (Gp. 1) and those who had been exposed  
117 to cold (8 °C), either before conception (Gp. 2), before conception and during the first  
118 week of gestation (Gp. 3) or before conception and during week one and two of  
119 gestation (Gp. 4) (**Fig. 1c**). Interestingly, we observed that offspring from parents that  
120 were exposed to cold before conception showed higher UCP1 expression both in iBAT  
121 and in ingWAT under regular housing conditions (RT) (**Fig. 1d**). When we challenged  
122 offspring by CE, the effect on UCP1 expression was markedly enhanced (**Fig. 1e** and  
123 **Supplementary Fig. 1e**). Taken together, our data indicate that CE of parents before  
124 conception or during gestation results in higher basal and stimulated UCP1 expression  
125 in the iBAT and ingWAT of the offspring.

## 126

### 127 **The effects of pre-conception cold exposure are mediated through the paternal** 128 **lineage**

129 Based on these findings, we analyzed whether the observed effect of CE was  
130 transmitted through the paternal (P-CE) or maternal (M-CE) lineage, focusing on the  
131 preconception exposure model in all subsequent studies. Intriguingly, we observed that  
132 the effects of parental CE on UCP1 expression at RT were mediated by the paternal  
133 lineage (**Fig. 2a**) and that the effect was enhanced in male iBAT and ingWAT and in  
134 female iBAT offspring when stimulated by CE (**Fig. 2b** and **Supplementary Fig. 2a**).  
135 Also, we could show that offspring from P-CE had higher UCP1 protein level than control  
136 (Ctrl) males at 21 days of age at RT and under thermoneutral (TN) conditions  
137 (**Supplementary Fig. 2b,c**). Analysis of gene expression in iBAT of P-CE offspring  
138 demonstrated higher mRNA expression of several markers of brown fat function in iBAT  
139 (**Fig. 2c**). We did not observe any changes in litter size and in nursing percentage over

140 the postnatal period (**Supplementary Fig. 2d,e**), suggesting that alterations in maternal  
141 behavior are not the cause for the observed phenotype. To exclude paternal behavior as  
142 a confounding factor, we performed *in vitro* fertilization (IVF) with sperm derived from P-  
143 CE or Ctrl males. We observed an induction of brown fat marker expression  
144 (**Supplementary Fig. 2f**) and UCP1 protein (**Fig. 2d** and **Supplementary Fig. 2g**) in  
145 iBAT of male and female P-CE vs Ctrl offspring, paralleled by a difference in body  
146 surface temperature (**Supplementary Fig. 2h**).

147 Since brown fat is formed at day E15.5 (ref. 24), we analyzed whether the  
148 observed changes were already present before birth. We could show that in iBAT from  
149 E18.5 embryos, *Ucp1* mRNA and other brown fat markers were higher (**Supplementary**  
150 **Fig. 2i**). Interestingly, these changes did not translate into an altered birth weight, nor  
151 did we observe differences in postnatal weight gain (**Supplementary Fig. 2j**). However,  
152 iBAT weight in 7-week old animals was significantly higher (**Supplementary Fig. 2k**),  
153 suggesting that not only expression of UCP1, but also the formation of iBAT is enhanced  
154 in P-CE offspring. In line with this, we could show by immunohistochemical analysis of  
155 iBAT and ingWAT that the area of UCP1<sup>+</sup> patches, denoting cells with high levels of  
156 UCP1 expression, was higher at RT in both iBAT and ingWAT (**Fig. 2e,f**). Upon CE, this  
157 phenotype was enhanced in both iBAT and ingWAT (**Fig. 2g,h**). We also observed lower  
158 lipid droplet size in ingWAT of P-CE offspring, suggesting a more active lipid metabolism  
159 (**Supplementary Fig. 2l**). Furthermore, reduced adipocyte size and more UCP1<sup>+</sup> cells  
160 were observed in P-CE offspring at 21 days of age at RT or at TN (**Supplementary Fig.**  
161 **2m-o**). Taken together, our data demonstrate that the effect of CE is mediated through  
162 the paternal lineage and affects both UCP1 expression and adipose tissue morphology.

163



164 **P-CE induces iBAT activity and systemic metabolism in the offspring**

165 Based on these findings, we analyzed whether the effect of P-CE would translate into a  
166 higher thermogenic activity. Surface temperature was higher in P-CE offspring  
167 compared to Ctrl offspring at P7 (**Fig. 3a**) at RT. At 7 weeks of age, animals had the  
168 same body weight (**Supplementary Fig. 3a**) and the same surface temperature (**Fig.**  
169 **3b**) at RT while upon CE, P-CE offspring exhibited a higher surface temperature (**Fig.**  
170 **3b**). Furthermore, we observed that P-CE-derived offspring had an 11% higher  $VO_2$  and  
171  $VCO_2$  at RT, which was enhanced upon acute CE (**Fig. 3c** and **Supplementary Fig.**  
172 **3b**), while respiratory exchange ratio (RER) remained unchanged (**Supplementary Fig.**  
173 **3c**). As CE can lead to shivering, we quantified the induction of brown fat in response to  
174 an i.p. injection of ADRB3-agonist CL316,243 (CL). We observed higher UCP1 protein  
175 (**Fig. 3d**), higher  $VO_2$  and  $VCO_2$  levels (**Fig. 3e** and **Supplementary Fig. 3d**),  
176 concomitant with more UCP1<sup>+</sup> cells in iBAT (**Fig. 3f**) of P-CE mice. Of special interest,  
177 we could show a lower RER in P-CE offspring following CL injection, suggesting a  
178 preferred utilization of fatty acids (**Supplementary Fig. 3e**).

179 Based on these data we analyzed whether the changes in respiration could lead  
180 to altered systemic metabolism. We did not observe any changes in body weight  
181 between 7 and 18 weeks of age (**Supplementary Fig. 3f**) when P-CE and Ctrl offspring  
182 were fed a regular chow diet at RT. Similarly, we did not observe any change in food  
183 intake (**Supplementary Fig. 3g**), however we could show that P-CE offspring exhibited  
184 a significant reduction in basal glucose levels as well as a trend for improved insulin  
185 sensitivity (**Supplementary Fig. 3h**). Insulin, cholesterol and fibroblast growth factor 21  
186 (FGF21) levels were the same (**Supplementary Fig. 3i-k**), and P-CE offspring showed  
187 lower circulating triacylglycerol (TAG) levels (**Supplementary Fig. 3l**) and higher

188 circulating non-esterified fatty acids (NEFAs) under fasted conditions (**Fig. 3g**). To  
189 assess whether the changes in altered glucose homeostasis could be due to a higher  
190 glucose uptake into iBAT, we injected Ctrl and P-CE offspring at RT or after CE with  
191 radiolabeled 2-deoxy-glucose. We observed higher glucose uptake exclusively into iBAT  
192 and ingWAT of P-CE offspring while muscle, brain, liver and heart glucose uptake was  
193 not affected (**Fig. 3h** and **Supplementary Fig. 3m**). These changes were paralleled by  
194 an induction of facilitated glucose transporter member 4 (GLUT4) expression in iBAT  
195 under CE (**Fig. 3i**). Taken together, our data demonstrate that P-CE induces brown and  
196 brite adipocyte function in the offspring, which leads to an improved systemic  
197 metabolism.

198

### 199 **The effect of P-CE is mediated in part through brown and brite adipocytes**

200 As several tissues contribute to the maintenance of body temperature, we next aimed to  
201 assess the contribution of brown and brite adipocytes. Therefore, we employed a  
202 transgenic mouse line, which expresses a diphtheria toxin receptor (DTR)- green  
203 fluorescent protein (GFP) fusion protein under the control of the *Ucp1* promoter (Ucp1-  
204 DTR-GFP mice)<sup>25</sup>. Sequential injections of diphtheria toxin A (DTA) in these mice leads  
205 to the complete ablation of brown adipocytes, indicated by the reduction in iBAT mass  
206 (**Fig. 4a**) and loss of UCP1 protein expression in iBAT (**Fig. 4b,c**). Similar to P-CE wild  
207 type mice, P-CE offspring from the Ucp1-DTR-GFP line exhibited slightly higher  $VO_2$   
208 and  $VCO_2$  at RT and a significant induction of both parameters upon CE at time point I  
209 (TP I) (**Fig. 4d** and **Supplementary Fig. 4a, TP I**). When mice were treated with DTA  
210 (TP II-IV), we observed a reduction in  $VO_2$  and  $VCO_2$  exclusively in P-CE offspring (**Fig.**  
211 **4d** and **Supplementary Fig. 4a, TP II-IV**) which, after three consecutive injections of

212 DTA, led to the abrogation of the difference in  $VO_2$  and  $VCO_2$ . The RER was not altered  
213 between the two groups at any time point (**Supplementary Fig. 4b**).

214 To avoid a shivering response in mice that received DTA injections, we analyzed  
215 respiration in animals in response to CL injections. We observed higher  $VO_2$  and  $VCO_2$   
216 in P-CE vs. Ctrl offspring of Ucp1-DTR-GFP mice after CL treatment (**Fig. 4e** and  
217 **Supplementary Fig. 4c, TP I**). As the CL injections caused only a transient increase in  
218 respiration, we treated the animals by three subsequent injections with CL and DTA  
219 (**Fig. 4e** and **Supplementary Fig. 4c, TP II-IV**). Already after two injections with DTA the  
220 difference between P-CE and Ctrl offspring on both  $VO_2$  and  $VCO_2$  was lost, suggesting  
221 that brown and brite adipocytes might be in part responsible for the observed higher  
222 respiration in P-CE-derived offspring. Similarly, we observed a lower RER in P-CE-  
223 derived offspring after CL injection, which was lost after DTA injection (**Supplementary**  
224 **Fig. 4d**). These findings were supported by the observation that 24 hours after the third  
225 CL+DTA injection, we did not observe any difference in respiration between both groups  
226 (**Fig. 4f** and **Supplementary Fig. 4e,f**). To analyze whether the observed effects would  
227 also translate into an induction of thermogenesis, we quantified surface temperature  
228 after an injection of either CL, with or without DTA mediated ablation of brown  
229 adipocytes. In accordance with previous data (**Fig. 4e**), surface temperature was higher  
230 in P-CE vs. Ctrl offspring after CL injection (**Fig. 4g**), and the effect was lost when brown  
231 adipocytes were ablated (**Fig. 4h**). Lastly, we could show that DTA injection did not  
232 induce overt inflammation in mice (**Supplementary Fig. 4g**). Taken together, our data  
233 demonstrate that the effect of P-CE on respiration and thermogenesis is at least in part  
234 mediated through the activation of brown adipocytes.

235

236 **P-CE protects from diet-induced obesity and insulin resistance**

237 As BAT has been implicated in energy expenditure, we aimed to assess whether body  
238 weight and metabolism would be different under challenged conditions. Therefore, we  
239 fed P-CE and Ctrl offspring a high-fat diet (HFD), with 60% of the calories derived from  
240 fat, for 10 weeks. Even though P-CE offspring consumed significantly more food than  
241 Ctrl offspring (**Fig. 5a**), we found that P-CE-derived offspring exhibited a slightly lower  
242 body weight gain and reduced fat mass compared to Ctrl (**Fig. 5b,c**). Furthermore, we  
243 could show that P-CE offspring had markedly better insulin sensitivity (**Fig. 5d**), even  
244 though fasting blood glucose levels were unchanged. The latter might be due to the  
245 lower levels of circulating insulin in P-CE offspring (**Fig. 5e**). We found significantly lower  
246 levels of circulating TAGs in P-CE vs. Ctrl offspring (**Fig. 5f**), while cholesterol levels  
247 remained unchanged (**Fig. 5g**).

248 Intriguingly, we observed a significantly higher metabolic rate indicated by higher  
249  $VO_2$  and  $VCO_2$  levels at RT conditions in P-CE vs Ctrl offspring (**Fig. 5h** and  
250 **Supplementary Fig. 5a**), while we did not observe any changes in substrate utilization,  
251 as indicated by an unchanged RER (**Supplementary Fig. 5b**). This higher oxygen  
252 consumption rate (OCR) was paralleled by significantly higher body surface temperature  
253 (**Supplementary Fig. 5c**) and UCP1 expression in iBAT (**Supplementary Fig. 5d**).  
254 Furthermore, we could show that hepatic lipid accumulation was reduced in P-CE vs.  
255 Ctrl offspring (**Fig. 5i,j**), which might explain the altered insulin sensitivity. Notably,  
256 circulating levels of FGF21, a hormone which has been suggested to be secreted from  
257 activated BAT<sup>26</sup> and is known to affect glucose and lipid homeostasis, was higher in P-  
258 CE offspring kept on a high fat diet (**Fig. 5k**). Taken together, our data demonstrate that

259 under RT conditions, which give mild cold stress, P-CE offspring are partially protected  
260 from diet induced obesity and maintain an improved metabolic profile.

261  
262 **Gene expression and DNA methylation analysis of P-CE offspring suggests**  
263 **changes in brown adipocyte formation and neurogenesis**

264 Based on our data, we asked whether transcriptional changes in iBAT could explain the  
265 observed phenotype. Therefore, we performed RNA sequencing (RNA-seq) of iBAT  
266 from P-CE and Ctrl offspring at RT and after a 3-day CE. Unbiased hierarchical  
267 clustering including all genes expressed in at least one sample group revealed distinct  
268 transcriptional profile of the different conditions (**Supplementary Fig. 6a**). A principal  
269 component (PC) analysis similarly showed distinct clusters of each of the 4 sample  
270 groups (**Fig. 6a**). PC1 appeared to capture differences imposed by acute cold exposure.  
271 Several genes related to BAT activity, such as glycerol kinase (*Gyk*) or *Ucp1* were major  
272 contributors of negative PC1 loadings, while muscle specific genes contributed to  
273 positive PC1 loadings. Interestingly, samples from P-CE offspring after CE had an even  
274 stronger negative PC1 loading than the Ctrl samples, indicating a hyperactivated BAT  
275 condition in P-CE offspring.

276 A pairwise differential gene expression analysis comparing Ctrl-RT vs. Ctrl-CE,  
277 considering significant hits with at least a 2-fold mean expression difference  
278 (**Supplementary Table 1**), identified many genes related to BAT activity  
279 (**Supplementary Fig. 6b,c**). In line with the PC analysis, we also found a number of  
280 genes upregulated in the CE samples from P-CE offspring compared to Ctrl offspring  
281 related to BAT activity (**Fig. 6b**) and an enrichment of gene ontology (GO) terms related  
282 to high metabolic activity in all significantly regulated genes (**Fig. 6c**). Of note, *Adrb3*

283 and *Ucp1* were also significantly differentially expressed, however the regulation was  
284 <2-fold between P-CE-CE and Ctrl-CE, therefore these genes were not included in the  
285 GO analysis.

286 As phenotypic and transcriptional changes of P-CE in the offspring are mediated  
287 through the sperm via the paternal lineage, we performed whole-genome bisulphite  
288 sequencing of sperm (6-fold average genomic coverage in each sample) to identify  
289 possible DNA methylation alterations which could potentially mediate the  
290 intergenerational transmission of the observed phenotype (**Fig. 6d**). We observed a  
291 small but significantly greater degree of global 5'-cytosine-phosphate-guanine-3' (CpG)  
292 DNA methylation in the P-CE samples (89.5% vs 87.5%; *P*-value < 0.002; **Fig. 6e**),  
293 indicating an effect of cold exposure on the sperm methylome.

294 To analyze whether methylation levels were altered in genomic regions which  
295 might affect gene expression in the offspring, we first performed hierarchical clustering  
296 and PC analysis of the methylation status of all promoter regions (**Fig. 6f** and  
297 **Supplementary Fig. 6d**). We observed a clear separation between P-CE and Ctrl  
298 sperm samples and a distinguishable clustering of the two groups in the PC analysis. In  
299 contrast to global CpG methylation, we found a small, but significant reduction in the  
300 average methylation levels of CpG islands (CGI) in P-CE samples (**Supplementary Fig.**  
301 **6e**). Hierarchical clustering and PC analysis of all non-CGI promoters showed  
302 comparable levels of separation on PC1 but less clear clustering, suggesting that the  
303 differences in CGI methylation are relevant contributors to the observed differences in  
304 promoter methylation.

305 These analyses indicate that the cold exposure induced methylation changes in  
306 sperm are reproducible and contribute to the observed phenotypic differences in the

307 offspring. It is important to note that sperm is a haploid cell type and as such, single CpG  
308 sites can only be either methylated or unmethylated. To address this issue, we decided  
309 to subdivide the genome in probes of 50 adjacent CpGs and analyze methylation  
310 changes over these probes. An unbiased analysis of the P-CE and Ctrl sperm  
311 methylome datasets identified 2431 DMRs with an overlapping or downstream (max.  
312 2kbp) gene (**Fig. 6g** and **Supplementary Table 2**). GO enrichment analysis of DMRs  
313 hypomethylated in P-CE samples related to many “neurogenesis” terms (**Fig. 6g**). A  
314 specific analysis of *Adrb3*, an important regulator of BAT activity, revealed local  
315 hypomethylation in the coding region (False discovery rate (FDR) = 0.01). An  
316 independent pyrosequencing analysis of individual CpG sites at the *Adrb3* locus in  
317 sperm samples confirmed this result (**Supplementary Fig. 6f**) and showed that the  
318 CpGs at the *Adrb3* locus were hypomethylated in adult iBAT and ingWAT from P-CE  
319 animals (**Supplementary Fig. 6g,h**). Interestingly, the transcriptomic analysis had  
320 shown that *Adrb3* was also significantly higher expressed in P-CE iBAT (**Fig. 2c** and **Fig.**  
321 **6b**). To test whether this effect was mediated by DNA methylation, we generated an  
322 *Adrb3* overexpression plasmid with a CpG-free backbone and in vitro methylated all  
323 CpGs. We then transfected the methylated and non-methylated plasmids into cells not  
324 expressing *Adrb3* (**Supplementary Fig. 6i**) and confirmed the methylation status of the  
325 CpG sites in the transfected plasmids (**Supplementary Fig. 6j**). We found that  
326 expression of *Adrb3* from the methylated plasmid was significantly lower than from the  
327 unmethylated plasmid, suggesting that DNA methylation at the *Adrb3* locus influences  
328 *Adrb3* expression.

329         Next, we elucidated whether the differential methylation status in the sperm of P-  
330 CE and Ctrl samples was directly correlated with transcriptional changes in iBAT tissue.

331 Therefore, we analyzed the expression levels of genes overlapping with DMRs either  
332 hypermethylated or hypomethylated in P-CE sperm. Interestingly we found that the  
333 average expression levels of transcripts overlapping with hypermethylated sperm P-CE  
334 DMRs were significantly increased compared to all transcripts, while inversely,  
335 transcripts overlapping with hypomethylated DMRs were significantly lower expressed in  
336 iBAT tissue (**Fig. 6h**). Gene body methylation is a feature of transcribed genes, even  
337 though the exact functions are not known<sup>27,28</sup>, and it is therefore possible that the  
338 identified sperm DMRs could contribute to the greater formation of iBAT tissue in P-CE  
339 animals, and might contribute to the observed intergenerational effect. We also found a  
340 number of transcripts being significantly differentially expressed (DE) in the iBAT of P-  
341 CE vs Ctrl CE samples and overlapping with hypo- or hypermethylated DMRs in the  
342 respective sperm samples, highlighting a potential direct effect of germline methylation  
343 levels and iBAT expression levels for selected genes (**Fig. 6i**). Taken together, our  
344 analyses support our findings that iBAT from P-CE mice is hyper-activated and in part  
345 dependent on enhanced brown adipocyte formation, reflected by the upregulated brown  
346 markers and downregulated muscle specific genes, possibly due to increased neuronal  
347 innervation.

348

#### 349 **P-CE leads to a cell autonomous increase in brown adipocyte formation**

350 To assess whether brown adipocyte formation is indeed altered in P-CE offspring, we  
351 isolated stromal vascular fraction (SVF) from iBAT of P-CE and Ctrl mice and  
352 differentiated these cells into mature brown adipocytes, *ex vivo*. When we analyzed lipid  
353 droplet staining, we did not observe any differences in either cell numbers or the  
354 appearance of multilocular cells (**Supplementary Fig. 7a-c**). However, we observed a



355 significant increase in the percentage of UCP1-positive cells, but not the average  
356 intensity of UCP1 staining in UCP1<sup>+</sup> cells (**Supplementary Fig. 7a,d,e**), suggesting an  
357 increased propensity to form brown adipocytes. We observed a significant induction of  
358 UCP1 protein and mRNA in P-CE offspring derived cells (**Supplementary Fig. 7f,g**).  
359 Similar to UCP1 we observed a higher *Adrb3* and cell death-inducing DFFA-like effector  
360 a (*Cidea*) mRNA expression, while peroxisome proliferator-activated receptor  $\gamma$  (*Ppar $\gamma$* )  
361 levels were the same (**Supplementary Fig. 7h-j**).

362 To analyze whether these changes would translate into altered functionality, we  
363 quantified the OCR of these *ex vivo* differentiated cells. While we did not observe any  
364 changes in basal OCR, we could show that cells from P-CE offspring had a significantly  
365 higher OCR under CL stimulated conditions (**Supplementary Fig. 7k**).

366 To confirm these findings, we quantified ADRB3 protein levels in P-CE and Ctrl  
367 offspring. In accordance with the mRNA data, we observed a higher ADRB3 protein  
368 expression in P-CE vs. Ctrl offspring at RT, CE and TN conditions (**Supplementary Fig.**  
369 **7l**). Given the widespread expression of *Adrb3* we also analyzed expression in ingWAT,  
370 epididymal adipose tissue (epiWAT) and heart (**Supplementary Fig. 7m**) and could  
371 show an up-regulation of *Adrb3* mRNA expression in ingWAT and epiWAT, but not in  
372 heart. To analyze whether this regulation could be connected to the DMR pattern which  
373 suggested an alteration in neurogenesis related genes, we analyzed tyrosine  
374 hydroxylase (TH) expression in iBAT from P-CE vs. Ctrl offspring, which was increased  
375 at both RT and after 2 days CE (**Supplementary Fig. 8a**) and we observed higher TH-  
376 immunostaining in neuronal axons within iBAT (**Supplementary Fig. 8b,c**). We checked  
377 vascularization by staining with isolectin B4 (IB4) and could show that iBAT from P-CE  
378 offspring was enriched with blood vessels (**Supplementary Fig. 8d,e**). These data

379 suggest that iBAT from P-CE offspring is more densely innervated and vascularized,  
380 which could explain the hyper-active state.

381 To test this hypothesis at a functional level, we performed microdialysis of iBAT  
382 from P-CE and Ctrl offspring. We observed an increased release of norepinephrine in P-  
383 CE offspring in response to a cold stimulus (**Supplementary Fig. 8f**). Furthermore,  
384 when we blocked adrenergic signaling *in vivo*, either with a selective ADRB3-antagonist  
385 L748,337 or an unspecific beta-blocker propranolol prior to CE, we observed that similar  
386 to BAT ablation, pretreatment with L748,337 or propranolol blocked the effect of P-CE  
387 on OCR (**Supplementary Fig. 8g,h**). Taken together, these data demonstrate that P-CE  
388 leads to higher neuronal innervation and norepinephrine release in iBAT of P-CE-  
389 derived offspring, while blocking beta-adrenergic receptor signaling in general, or  
390 ADRB3 in particular, abrogates the effect of P-CE.

391

## 392 **Discussion**

393 Paternal adaptation to environmental cues have been linked to various physiological  
394 changes in the offspring utilizing different animal model systems<sup>22,29</sup>. Our data indicate  
395 that CE can be a determinant of the offspring's physiology. This finding is in line with a  
396 recent study suggesting that seasonality can affect systemic metabolism<sup>23,30-33</sup> and that  
397 temperature sensing might influence physiological adaptation. A possible implication for  
398 clinical weight-loss studies could be randomization stratified by birth season, however  
399 such a mechanism would have to be investigated in a prospective trial. Furthermore,  
400 despite the large number of individuals studied in our cohort and the low *P*-value, our  
401 results still need to be interpreted with caution. First, the retrospective nature of the  
402 study and the inclusion of individuals undergoing FDG-PET/CT introduces numerous

403 biases. Since BAT was not specifically stimulated, an unknown proportion of “BAT-  
404 negative” labelled individuals may still have functional but inactive BAT. Second, the  
405 location of birth and conception are unknown, which is problematic as there were at  
406 least two major immigration waves to Switzerland from southern parts of Europe in the  
407 past century<sup>34</sup>. Third, the climate in Switzerland varies significantly ranging from a mild,  
408 Mediterranean-like climate to arctic conditions. Moreover, the clothing style of individuals  
409 may not always correlate with the absolute outside temperature, but rather with the  
410 perceived meteorological season. Lastly, the amount of daylight has been shown to  
411 negatively correlate with BAT activation<sup>35</sup> and is an inseparable confounder in this kind  
412 of retrospective cohort study.

413         Based on our data we propose that pre-conception CE of male mice leads to a  
414 higher degree of inducibility of brown fat which is in line with previous work  
415 demonstrating that seminal plasma can be the carrier for phenotypic alterations<sup>36</sup>. A  
416 possible explanation for the lack of transmission via the maternal lineage is the  
417 anatomical location of testis, which is directly exposed to changes in temperature<sup>37</sup>.  
418 Nevertheless, it remains unclear whether sperm directly senses temperature or whether  
419 the effect is due to a signal derived from other cells. While *de novo* methylation is  
420 initiated around E13.5 in mitotically arrested prospermatogonia and the methylome is  
421 completely established prior to birth, *de novo* methylation is not initiated until after birth  
422 in the female germline. As a result, the sperm methylome is dependent on faithful DNA  
423 methylation maintenance while the oocyte methylome is purely reflective of *de novo*  
424 methylation events. Furthermore, it should be noted that CE does generally not have the  
425 capacity to promote genetic mutations; therefore, the observed phenomenon is not  
426 driven by genetic inheritance but by (environmental) epigenetic inheritance.

427           The observed relative increase in basal brown fat UCP1 protein expression at RT  
428 in P-CE offspring might be due to the fact that 23°C constitutes a mild cold challenge to  
429 mice<sup>38</sup>. The observed reduction in circulating triacylglycerols (TAGs) is in line with a  
430 previous report demonstrating that BAT is a major sink for TAGs<sup>39</sup>, while the higher  
431 NEFA levels during fasting in P-CE vs Ctrl mice could be due to enhanced Adrb3  
432 signaling in white adipose tissue.

433           Multiple studies have implicated that BAT plays an important role in metabolism,  
434 however, very few studies have quantified the actual contribution of BAT. Since *Ucp1*  
435 deletion requires breeding and housing at TN, use of *Ucp1*-ko mice might influence the  
436 physiological response<sup>40</sup>. By using an acute model of DTA targeted ablation exclusive to  
437 brown and active brite adipocytes<sup>25</sup>, we were able to show that BAT at least in part  
438 mediates the observed metabolic changes, even though changes in heart, white fat or in  
439 inflammatory responses could account for parts of the metabolic alterations.

440           Based on our results, we propose that paternal cold induces a hyperactive state  
441 in brown adipose tissue of the offspring, which leads to improved adaptation to  
442 overnutrition and hypothermia. Various DMRs did overlap with or are in close proximity  
443 to genes annotated for neurogenesis. Furthermore, the observed denser neuronal  
444 innervation, higher vascularization and increased norepinephrine release in iBAT<sup>41</sup>,  
445 highlight that multiple genes contribute to this complex phenotype. Together these  
446 results suggest the CE affects the sperm methylome, raising the possibility that altered  
447 sperm DNA methylation in CE fathers contributes to the observed phenotype. It is worth  
448 noting that this is, to our knowledge, the first example in which adult CE leads to  
449 significant alterations in sperm methylation. While recent studies have shown that  
450 "epivariation", i.e. stochastic individual differences in DNA methylation, can be the major

451 contributor to the sperm methylome<sup>42</sup>, we would like to point out that the significant  
452 concordant global methylation changes, as well as the clear separation of promoter  
453 methylation profiles in sperm of P-CE mice vs. Ctrl animals, suggest a direct effect of CE  
454 on the sperm methylome. Nonetheless, whether these modifications are causative or  
455 whether other epigenetic modifications, which can convey inherited traits<sup>43</sup>, such as  
456 histone modifications<sup>44</sup> or long non-coding and small RNAs<sup>45</sup> contribute to the observed  
457 phenotype, remains to be analyzed.

458         The phenomenon identified here may also have implications for evolutionary  
459 biology as adaptation to environmental temperature changes is critical for any organism.  
460 Intergenerational memory of past CEs, may have been one mechanism to improve the  
461 survival of the offspring, during prolonged phases of cold exposure, such as the ice age  
462 2.6 million years ago. In conclusion, through modulation of genetic and epigenetic  
463 variances, environmental changes might influence adipose tissue and metabolism not  
464 only in the exposed individual but also in the next generation. Such mechanisms might  
465 be exploitable to design therapies and personalized strategies to induce BAT  
466 functionality to counteract obesity and co-morbidity diseases.

467

## 468 **Acknowledgements**

469 We are grateful to M. Stoffel, J. Krützfeldt and members of the Wolfrum lab for helpful  
470 discussion. We would also like to thank K. Tabbada for assistance with WGBS high-  
471 throughput sequencing and F. Krueger and S. Andrews for help with bioinformatics  
472 analysis. We thank K. De Bock and F. Zheng for IB4 antibody. We thank K.A. Rollins for  
473 editing the manuscript. Data produced and analyzed in this paper were generated in  
474 collaboration with the Genetic Diversity Centre (GDC) and Functional Genomics Center

475 Zurich (FGCZ). The work was supported by the Swiss National Science Foundation  
476 (SNSF, CW and FvM).

477

#### 478 **Author Contributions**

479 W.S. and C.W. designed the study. W.S. and H.D. performed all experimental work  
480 except the following. P.P. performed IVF. S.M. helped with the seahorse experiments.  
481 D.H.D. performed the Ucp1-DTR-GFP mice characterization. C.W., V.E., M.B., and  
482 D.H.D. contributed to radio labeled glucose tracing. E.K. did paraffin sectioning. G.G. did  
483 lipid droplet size quantification. A.P. helped with FACS. V.E. performed automated  
484 image analysis. L.G.S. helped with indirect calorimetry analysis. G.S. helped in the  
485 analysis of maternal behavior. D.P.-R. and W.S. did the microdialysis studies. A.S.B.,  
486 I.A.B., S.B. and C.Z. carried out the retrospective analysis of BAT in humans. W.S and  
487 C.W wrote the manuscript. L.O. contributed to RNA-seq data analysis. F.v.M. and W.R.  
488 did DNA methylation sequencing and bioinformatic analysis. F.v.M, A.S.B., I.A.B.,  
489 D.H.D., S.M., M.B. and L.B. helped with manuscript editing.

490

#### 491 **Conflict of Financial Interests statement**

492 The authors have NO affiliations with or involvement in any organization or entity with  
493 any financial interest or non-financial interest in the subject matter or materials  
494 discussed in this manuscript.

495 **References**

- 496 1. WHO. Obesity and overweight Fact sheet. (2018).
- 497 2. Rosen, E.D. & Spiegelman, B.M. What we talk about when we talk about fat. *Cell* **156**,  
498 20-44 (2014).
- 499 3. Tseng, Y.H., Cypess, A.M. & Kahn, C.R. Cellular bioenergetics as a target for obesity  
500 therapy. *Nat Rev Drug Discov* **9**, 465-482 (2010).
- 501 4. Frontini, A. & Cinti, S. Distribution and development of brown adipocytes in the murine  
502 and human adipose organ. *Cell Metab* **11**, 253-256 (2010).
- 503 5. Bartelt, A. & Heeren, J. Adipose tissue browning and metabolic health. *Nat Rev*  
504 *Endocrinol* **10**, 24-36 (2014).
- 505 6. Cannon, B. & Nedergaard, J. Brown adipose tissue: function and physiological  
506 significance. *Physiological reviews* **84**, 277-359 (2004).
- 507 7. Rosenwald M, W.C. The origin and definition of brite versus white and classical brown  
508 adipocytes. . *Adipocyte* **30**, 1 (2013).
- 509 8. Hany, T.F., *et al.* Brown adipose tissue: a factor to consider in symmetrical tracer uptake  
510 in the neck and upper chest region. *European journal of nuclear medicine and molecular*  
511 *imaging* **29**, 1393-1398 (2002).
- 512 9. Cypess, A.M., *et al.* Identification and importance of brown adipose tissue in adult  
513 humans. *N Engl J Med* **360**, 1509-1517 (2009).
- 514 10. Saito, M., *et al.* High incidence of metabolically active brown adipose tissue in healthy  
515 adult humans: effects of cold exposure and adiposity. *Diabetes* **58**, 1526-1531 (2009).
- 516 11. van Marken Lichtenbelt, W.D., *et al.* Cold-activated brown adipose tissue in healthy men.  
517 *N Engl J Med* **360**, 1500-1508 (2009).
- 518 12. Virtanen, K.A., *et al.* Functional brown adipose tissue in healthy adults. *The New England*  
519 *journal of medicine* **360**, 1518-1525 (2009).
- 520 13. Zingaretti, M.C., *et al.* The presence of UCP1 demonstrates that metabolically active  
521 adipose tissue in the neck of adult humans truly represents brown adipose tissue.  
522 *FASEB J* (2009).
- 523 14. Nedergaard, J., Bengtsson, T. & Cannon, B. Unexpected evidence for active brown  
524 adipose tissue in adult humans. *Am J Physiol Endocrinol Metab* **293**, E444-452 (2007).
- 525 15. Cypess, A.M., *et al.* Activation of human brown adipose tissue by a beta3-adrenergic  
526 receptor agonist. *Cell Metab* **21**, 33-38 (2015).
- 527 16. Yoneshiro, T., *et al.* Recruited brown adipose tissue as an antiobesity agent in humans. *J*  
528 *Clin Invest* **123**, 3404-3408 (2013).
- 529 17. Carone, B.R., *et al.* Paternally induced transgenerational environmental reprogramming  
530 of metabolic gene expression in mammals. *Cell* **143**, 1084-1096 (2010).

- 531 18. Ng, S.F., *et al.* Chronic high-fat diet in fathers programs beta-cell dysfunction in female  
532 rat offspring. *Nature* **467**, 963-966 (2010).
- 533 19. Jaenisch, R. & Bird, A. Epigenetic regulation of gene expression: how the genome  
534 integrates intrinsic and environmental signals. *Nat Genet* **33 Suppl**, 245-254 (2003).
- 535 20. Seong, K.H., Li, D., Shimizu, H., Nakamura, R. & Ishii, S. Inheritance of stress-induced,  
536 ATF-2-dependent epigenetic change. *Cell* **145**, 1049-1061 (2011).
- 537 21. Anderson, L.M., *et al.* Preconceptional fasting of fathers alters serum glucose in offspring  
538 of mice. *Nutrition* **22**, 327-331 (2006).
- 539 22. Ng, S.F., *et al.* Paternal high-fat diet consumption induces common changes in the  
540 transcriptomes of retroperitoneal adipose and pancreatic islet tissues in female rat  
541 offspring. *FASEB J* **28**, 1830-1841 (2014).
- 542 23. Phillips, D.I. & Young, J.B. Birth weight, climate at birth and the risk of obesity in adult  
543 life. *Int J Obes Relat Metab Disord* **24**, 281-287 (2000).
- 544 24. Kaufman, M.H. <<The>> *atlas of mouse development*, (Academic Press, London <etc.>,  
545 1994).
- 546 25. Rosenwald, M., Perdikari, A., Rulicke, T. & Wolfrum, C. Bi-directional interconversion of  
547 brite and white adipocytes. *Nat Cell Biol* **15**, 659-667 (2013).
- 548 26. Hondares, E., *et al.* Thermogenic activation induces FGF21 expression and release in  
549 brown adipose tissue. *J Biol Chem* **286**, 12983-12990 (2011).
- 550 27. Jones, P.A. Functions of DNA methylation: islands, start sites, gene bodies and beyond.  
551 *Nature reviews. Genetics* **13**, 484-492 (2012).
- 552 28. Yang, X., *et al.* Gene body methylation can alter gene expression and is a therapeutic  
553 target in cancer. *Cancer Cell* **26**, 577-590 (2014).
- 554 29. Ost, A., *et al.* Paternal diet defines offspring chromatin state and intergenerational  
555 obesity. *Cell* **159**, 1352-1364 (2014).
- 556 30. Lv, J., *et al.* The associations of month of birth with body mass index, waist  
557 circumference, and leg length: findings from the China Kadoorie Biobank of 0.5 million  
558 adults. *J Epidemiol* **25**, 221-230 (2015).
- 559 31. Speakman, J.R. & Heidari-Bakavoli, S. Type 2 diabetes, but not obesity, prevalence is  
560 positively associated with ambient temperature. *Sci Rep* **6**, 30409 (2016).
- 561 32. Valdes, S., *et al.* Ambient temperature and prevalence of obesity in the Spanish  
562 population: The Di@bet.es study. *Obesity (Silver Spring)* **22**, 2328-2332 (2014).
- 563 33. Yang, H.K., *et al.* Ambient Temperature and Prevalence of Obesity: A Nationwide  
564 Population-Based Study in Korea. *PLoS One* **10**, e0141724 (2015).
- 565 34. Afonso, A. *Immigration and its impacts in Switzerland*, (Duke Univ. Press, Washington  
566 DC, 2004).



- 567 35. Au-Yong, I.T.H., Thorn, N., Ganatra, R., Perkins, A.C. & Symonds, M.E. Brown Adipose  
568 Tissue and Seasonal Variation in Humans. *Diabetes* **58**, 2583-2587 (2009).
- 569 36. Adefuye, A.O., Sales, K.J. & Katz, A.A. Seminal plasma induces the expression of IL-  
570 1alpha in normal and neoplastic cervical cells via EP2/EGFR/PI3K/AKT pathway. *J Mol*  
571 *Signal* **9**, 8 (2014).
- 572 37. Zhang, Z., *et al.* Functional analysis of the cooled rat testis. *J Androl* **25**, 57-68 (2004).
- 573 38. Fischer, A.W., Cannon, B. & Nedergaard, J. Optimal housing temperatures for mice to  
574 mimic the thermal environment of humans: An experimental study. *Mol Metab* (2017).
- 575 39. Bartelt, A., *et al.* Brown adipose tissue activity controls triglyceride clearance. *Nat Med*  
576 **17**, 200-205 (2011).
- 577 40. Shabalina, I.G., *et al.* UCP1 in brite/beige adipose tissue mitochondria is functionally  
578 thermogenic. *Cell Rep* **5**, 1196-1203 (2013).
- 579 41. Bronnikov, G., Houstek, J. & Nedergaard, J. Beta-adrenergic, cAMP-mediated  
580 stimulation of proliferation of brown fat cells in primary culture. Mediation via beta 1 but  
581 not via beta 3 adrenoceptors. *J Biol Chem* **267**, 2006-2013 (1992).
- 582 42. Shea, J.M., *et al.* Genetic and Epigenetic Variation, but Not Diet, Shape the Sperm  
583 Methylome. *Dev Cell* **35**, 750-758 (2015).
- 584 43. Rando, O.J. Intergenerational Transfer of Epigenetic Information in Sperm. *Cold Spring*  
585 *Harb Perspect Med* **6**(2016).
- 586 44. Greer, E.L. & Shi, Y. Histone methylation: a dynamic mark in health, disease and  
587 inheritance. *Nature reviews. Genetics* **13**, 343-357 (2012).
- 588 45. Daxinger, L. & Whitelaw, E. Understanding transgenerational epigenetic inheritance via  
589 the gametes in mammals. *Nature reviews. Genetics* **13**, 153-162 (2012).

591 **Figure 1**

592 Parental cold exposure induces UCP1 expression in iBAT and ingWAT.

593 **(a)** The birthday frequency of individuals with no active BAT (no BAT) and active BAT  
594 (top panel) and the ratio of such individuals as a function of birth date (middle panel).

595 BAT activity is measured by FDG-PET/CT ( $n = 8440$  individuals,  $P = 1E-16$ ). Monthly  
596 mean temperatures in Switzerland (bottom panel), to serve as a visual illustration of the

597 warmer and colder periods. **(b)** BMI of BAT-negative (black boxes) and BAT-positive  
598 (green boxes) individuals born between April-September and October-March. Vertical

599 bars are estimated 95%-CI's, The middle line represents the median, the top and bottom  
600 line the 75th and 25th percentile, respectively, the whiskers have the length 1.5 x

601 interquartile range,  $n = 914$  individuals,  $P = 0.00091$ , two-sided  $t$ -test, Bonferroni-  
602 corrected. **(c)** Scheme for the parental cold exposure mouse model. 10-week male and

603 female C57BL/6 mice were cold stimulated for 0 (Group 1), 7 (Group 2), 14 (Group 3)  
604 and 21 days (Group 4) at 8 °C, then returned to 23 °C. Each block denotes 1 week;

605 breeding was initiated at the end of the block 1. **(d,e)** Cropped western blots of UCP1 ( $\gamma$ -  
606 tubulin is the loading control) in the 4 experimental groups of offspring described in **c**

607 from iBAT and ingWAT isolated while the mice were at RT **(d)** or after CE **(e)**. Shown is  
608 one representative blot from four independent experiments, graphs depict mean of litter

609 from all experiments  $\pm$  standard error of mean (SEM),  $n =$  number of litters tested, each  
610 dot represents one litter. Statistical significance was calculated using one-way analysis

611 of variance (ANOVA) test, **(d-left)**  $n = 7$ ,  $F_{(3,24)}=6.48$ ; **(d-right)**  $n = 8$ ,  $F_{(3,28)}=3.52$ ; **(e-left)**  
612  $n = 8$ ,  $F_{(3,28)}=10.90$ ; **(e-right)**  $n = 8$ ,  $F_{(3,28)}=8.65$ ; Results are reported as mean  $\pm$  SEM, \*

613  $P < 0.05$ , \*\*  $P < 0.01$ , \*\*\* $P < 0.001$ .

614

615 **Figure 2**

616 Paternal cold exposure exclusively induces UCP1 expression in iBAT and ingWAT

617 **(a,b)** Either female (M-CE) or male (P-CE) mice were cold stimulated for 7 days before  
618 initiating a mating. All mice were kept at 23 °C afterwards. **(a,b)** Cropped western blots  
619 of UCP1 ( $\gamma$ -tubulin and HSP90 are the loading controls) in the 3 experimental groups of  
620 offspring of Ctrl, M-CE, and P-CE from iBAT and ingWAT isolated while the mice were at  
621 RT **(a)** or after CE **(b)**. **(c)** mRNA levels of different brown fat markers in iBAT of Ctrl and  
622 P-CE offspring at RT,  $n = 8$  litters, normalized by  $\Delta$ Ct values. **(d)** Cropped western blots  
623 of UCP1 (HSP90 is the loading control) in the *IVF* offspring of Ctrl and P-CE from iBAT  
624 at RT and after 2 days CE, ( $n = 11$  litters for Ctrl and 10 litters for P-CE). **(e-h)**  
625 Representative H&E and UCP1 immunohistochemistry staining of **(e,g)** iBAT and **(f,h)**  
626 ingWAT, of Ctrl or P-CE offspring at **(e,f)** 23 °C and **(g,h)** 8 °C, scale bar 100  $\mu$ m,  $n =$   
627 litters per group. **(a-left)**  $n = 8$ ,  $F_{(2,21)} = 4.93$ ,  $P = 0.018$ ; **(a-right)**  $n = 8$ ,  $F_{(2,21)} = 3.92$ ,  $P =$   
628  $0.036$ ; **(b-left)**  $n = 7$ ,  $F_{(2,18)} = 8.27$ ,  $P = 0.003$ ; **(b-right)**  $n = 8$ ,  $F_{(2,21)} = 7.74$ ,  $P = 0.003$ ; **(d-**  
629 **left)**  $P = 0.003$ ; **(d-right)**  $P = 0.02$ . Throughout, data are mean  $\pm$  SEM, each dot  
630 represents one litter, \*  $P < 0.05$ , \*\*  $P < 0.01$ , and \*\*\* $P < 0.001$  by one-way analysis of  
631 variance (ANOVA) **(a,b)** or by two-tailed unpaired Student's *t*-test **(c,d)**.

632

633 **Figure 3**

634 Paternal cold exposure induces oxygen consumption in offspring upon cold or ADRB3-  
635 agonist stimulation

636 **(a)** Representative thermographic image of Ctrl and P-CE offspring at postnatal day 7.  
637 Offspring were kept at RT, right inset depicts calculated averages of surface  
638 temperature,  $n = 7$  litters,  $P = 0.04$ . **(b)** Representative thermographic image of Ctrl and

639 P-CE offspring at 23 °C and after 30h of CE,  $n = 7$  litters,  $P$  (30h CE) = 0.03. (c) Time  
640 resolved oxygen consumption in Ctrl and P-CE offspring mice, with cold induction  
641 (arrow) followed by warm adaption (arrow),  $P = 0.006$ , dark phase is marked as dark  
642 background, right inset depicts calculated means as indicated,  $n = 5$  litters. (d) Cropped  
643 western blots of UCP1 (HSP90 is the loading control) of iBAT from Ctrl and P-CE  
644 offspring, injected with saline or CL (0.1 mg/kg body weight, 3 times, every 24 h,  $n = 7$   
645 litters). (e) Time resolved Oxygen consumption of Ctrl ( $n = 4$  litters) and P-CE ( $n = 5$   
646 litters) offspring, with CL (arrow),  $P = 0.003$ . (f) Representative UCP1 staining of iBAT of  
647 Ctrl or P-CE offspring with CL injection, scale bar 100  $\mu\text{m}$ ,  $n = 6$  litters per group. (g)  
648 Serum NEFAs level of fasted (12h) and refeeding (4h) animals from Ctrl ( $n = 7$  litters)  
649 and P-CE ( $n = 8$  litters). (h) Glucose uptake in BAT at RT, 1 day and 3 days of CE ( $n = 7$   
650 litters for all groups, except  $n = 8$  for P-CE at RT and 1 day CE). (i) Western blots of  
651 GLUT4 (HSP90 is the loading control) of iBAT isolated from Ctrl or P-CE offspring at RT  
652 and after 3 days of CE,  $n = 4$  litters. Results are reported as mean  $\pm$  SEM, each dot  
653 represents one litter. Statistical significance was calculated using a two-tailed unpaired  
654 Student's  $t$ -test; \*  $P < 0.05$ , \*\*  $P < 0.01$ .

655

#### 656 **Figure 4**

657 Paternal cold exposure induces oxygen consumption in offspring due to increased BAT  
658 functionality

659 (a) Tissue wet weight ( $n = 4$  mice,  $P = 0.000001$ ) and (b) Cropped western blots of  
660 UCP1 ( $\gamma$ -tubulin is the loading control) of iBAT from Ucp1-DTR-GFP mice (11-weeks of  
661 age) with saline or diphtheria toxin A (DTA) injection. (c) Representative H&E and UCP1  
662 staining of iBAT of Ucp1-DTR-GFP animal after saline or DTA injection, scale bar, 100

663  $\mu\text{m}$ ,  $n = 4$  mice. **(d)** Time resolved oxygen consumption in Ucp1-DTR-GFP Ctrl ( $n = 4$   
664 litters) and P-CE ( $n = 5$  litters) offspring with cold induction (TP I) followed by three DTA  
665 injections (TP II-IV), light cycle (L), dark cycle (D) right inset depicts calculated means as  
666 indicated, dark phase is marked as dark background,  $P = 0.04$ . **(e)** Time resolved  
667 oxygen consumption in Ucp1-DTR-GFP Ctrl and P-CE offspring with CL injection (TP I)  
668 followed by three DTA+CL injections (TP II-IV), right inset depicts calculated mean as  
669 indicated,  $n = 4$  litters,  $P = 0.03$ . **(f)** Time resolved oxygen consumption in Ucp1-DTR-  
670 GFP Ctrl and P-CE offspring 24 hour after BAT depletion (TP IV, **e**) and stimulated with  
671 CL (arrow),  $n = 4$  litters. **(g, h)** Representative thermographic image of Ctrl and P-CE  
672 offspring with CL stimulation **(g)** before and **(h)** after BAT depletion, lower insets depict  
673 calculated averages,  $n = 8$  litters. Results are reported as mean  $\pm$  SEM. Statistical  
674 significance was calculated using a two-tailed unpaired Student's *t*-test; \*  $P < 0.05$ , \*\*\* $P$   
675  $< 0.001$ .

676

## 677 **Figure 5**

678 Paternal cold exposure protects offspring from high fat diet induced obesity

679 **(a-c)** Daily **(a)** food intake, **(b)** body weight gain and **(c)** body composition of Ctrl and P-  
680 CE offspring mice fed a high fat diet, at RT for the indicated time. **(a)**  $n = 12$ , **(b)**  $n = 11$ ,  
681 **(c)**  $n = 6$  **(d)** Insulin tolerance test of Ctrl or P-CE offspring fed a HFD for 7 weeks at RT,  
682 6h fasting,  $n = 12$ . Shown is one representative from three independent experiments. **(e-  
683 g)** Circulating **(e)** Insulin, **(f)** TAG and **(g)** Cholesterol levels of Ctrl or P-CE offspring fed  
684 a HFD for 11 weeks at RT. **(e)**  $n = 12$ , **(f)**  $n = 11$ , **(g)**  $n = 9$ . **(h)** Time resolved oxygen  
685 consumption time course and analysis, of Ctrl or P-CE offspring fed a HFD for 11 weeks  
686 at RT, right inset depicts calculated mean as indicated,  $n = 5$ ,  $P = 0.001$ . **(i)**

687 Representative Oil red O staining on liver sections, of Ctrl or P-CE offspring fed a HFD  
688 for 11 weeks at RT, scale bar 200  $\mu\text{m}$ ,  $n = 6$  litters. (j) TAG content in liver,  $n = 6$ . (k)  
689 Circulating FGF21 levels of Ctrl or P-CE offspring on HFD,  $n = 9$ . Results are reported  
690 as mean  $\pm$  SEM,  $n =$  number of litters tested, each dot represents one litter. Statistical  
691 significance was calculated using a two-tailed unpaired Student's  $t$ -test; \*  $P < 0.05$ , \*\*  $P$   
692  $< 0.01$ , \*\*\* $P < 0.001$ .

693

## 694 **Figure 6**

695 Paternal cold exposure affects the transcriptional signature of the brown adipose tissue  
696 in the offspring and the epigenetic profile of the sperm

697 (a) Principal component analysis (PCA) of RNA-seq data from brown adipose tissue  
698 (BAT) samples. PC1 and PC2 for each sample were calculated using the SeqMonk PCA  
699 analysis pipeline,  $n = 6$  litters. (b) Scatter plot of RNA-seq data from BAT samples,  
700 comparing P-CE vs CTRL samples following 3 days of cold exposure (3CE). Plotted are  
701 the  $\log_2$ -transformed normalized reads per million (RPM). Significant differentially  
702 expressed genes (overlap between DEseq2 and EdgeR) with at least 2-fold mean  
703 expression differences are highlighted in red. Selected genes of interest which do not  
704 fulfill all of the above criteria are labeled in blue and or only shown for comparison with  
705 the literature,  $n = 6$ . (c) GO terms of up and down regulated genes in P-CE-CE against  
706 Ctrl-CE samples,  $n = 6$  litters. (d) Heatmap showing the methylation levels in DMRs  
707 between P-CE and Ctrl sperm samples. Clustering of DMRs was performed in  
708 SeqMonk. (e) Box whisker plots showing the CpG methylation levels of individual  
709 replicates of sperm samples from P-CE and Ctrl samples. Methylation was quantitated  
710 over consecutive probes spanning 50 CpGs. Significance was calculated using the

711 mean CpG methylation levels of P-CE vs Ctrl samples using a two-tailed unpaired  
712 Students *t*-test,  $n = 6$  mice,  $P = 0.00052$ . (f) Hierarchical clustering of promoter CpG  
713 methylation levels. (g) GO terms of hyper and hypo DMRs in P-CE over RT sperm,  $n = 6$   
714 mice. (h) Expression levels of transcripts in BAT samples overlapping with sperm DMRs  
715 either hypermethylated or hypomethylated in the paternal cold exposure vs control  
716 samples. Shown are the log<sub>2</sub> RPM gene expression levels in BAT. Significance was  
717 calculated from the average gene expression levels of each group using a two-tailed  
718 unpaired Students *t*-test.  $n = 6$  mice, number of all expressed genes is 11334, number of  
719 genes overlapping P-CE Hypermethylated Sperm DMRs is 1049, number of genes  
720 overlapping P-CE Hypomethylated Sperm DMRs is 365, "All expressed genes" vs  
721 "Genes overlapping P-CE Hypermethylated Sperm DMRs":  $P = 3.7E-14$ , "All expressed  
722 genes" vs "Genes overlapping P-CE Hypomethylated Sperm DMRs":  $P = 1.4E-6$ . Any  
723 individual points that fall outside this range are shown as filled circles. Each circle  
724 represents a single probe. (i) Scatter plot of RNA-seq data from BAT samples,  
725 comparing P-CE vs CTRL samples following 3 days of cold exposure (3CE). Plotted are  
726 the log<sub>2</sub>-transformed normalized reads per million (RPM). Highlighted are all genes  
727 which are significant differentially expressed (overlap between DEseq2 and EdgeR with  
728 at least 2-fold mean expression differences) between P-CE-3CE and Ctrl-3CE samples  
729 and overlap with identified sperm DMRs. (e,h) box plots of the CpG methylation  
730 percentages of tiling probes spanning 50 CpGs each. The middle line indicates the  
731 median of the data, the upper and lower extremities of the box show the 25th and 75th  
732 percentiles, and the upper and lower black whiskers show the median  $\pm$  the interquartile  
733 range (25%–75%) multiplied by 2. \*\*\* $P < 0.001$ .

734 **CONTACT FOR REAGENT AND RESOURCE SHARING**

735 For further information and requests for reagents generated in this study, please contact

736 lead contact Christian Wolfrum ([christian-wolfrum@ethz.ch](mailto:christian-wolfrum@ethz.ch)).



## 737 **METHODS**

### 738 **Materials**

739 Details of the reagents used in this study are listed in Life Sciences Reporting Summary.

740

### 741 **Human study**

742 13502 <sup>18</sup>F-DG-PET/CT scans of 8440 individuals examined during Nov.-Feb. in the years  
743 2007 – 2015 were reviewed for the presence of active BAT by physicians<sup>46</sup>. Uptake in  
744 the supraclavicular and cervical area was considered grade 1, paravertebral, mediastinal  
745 grade 2 and infradiaphragmal grade 3. Readers were blinded to the hypothesis of this  
746 study. The birthdates of the individuals were extracted from the DICOM (Digital Imaging  
747 and Communications in Medicine) metadata of the images. Density plots of the birthdays  
748 were created with ggplot2 2.1.0 in R 3.3.1. (R Foundation for Statistical Computing,  
749 Vienna, Austria). The distributions of individuals were examined with a generalized linear  
750 model (Poisson error distribution and link function) to estimate the likelihood of being  
751 conceived in the cold period of the year. The BAT negative control cohort was matched  
752 for sex and age with the nearest neighbor algorithm<sup>47</sup>. The mean temperature of  
753 northern Switzerland was acquired from the federal meteorological in a monthly  
754 resolution. The study was approved by the Cantonal Ethics Committee Zürich.

755

### 756 **Mice**

757 C57BL/6N wild-type mice were obtained from Charles River. Ucp1-DTR-GFP mice were  
758 generated as described previously<sup>25</sup>. Unless indicated otherwise, all experiments were  
759 performed with adult male mice kept on an inverted 12h dark/light cycle, fed *ad libitum*

760 chow diet or 60% high fat diet. For cold stimulation, animals were housed in long type II  
761 cages at 8°C. All animal studies were approved by the Veterinäramt Zürich.

762

### 763 **Primary adipocyte culture/HEK 293 cell culture**

764 For cellular separation, dissected adipose tissues were minced with a scalpel blade and  
765 incubated in 2.0 ml/mg (wet tissue) 0.2% collagenase type II in collagenase buffer (25  
766 mM KHCO<sub>3</sub>, 12 mM KH<sub>2</sub>PO<sub>4</sub>, 1.2 mM MgSO<sub>4</sub>, 4.8 mM KCl, 120 NaCl, 1.2 mM CaCl<sub>2</sub>, 5  
767 mM glucose, 2.5% BSA, 1% Pen/Strep, pH 7.4) for 50 min at 37°C with occasional  
768 resuspension. 10 ml centrifugation buffer (70% PBS, 15% FBS, 15% HistoPaque 1119)  
769 was added and samples were centrifuged 5 min at 200 g. The SVF pellet from the initial  
770 centrifugation was resuspended in 2 ml erythrocyte lysis buffer (154 mM NH<sub>4</sub>Cl, 10 mM  
771 KHCO<sub>3</sub>, 0.1 mM EDTA, pH 7.4) and incubated for 4 min on ice. Samples were filtered  
772 through 40 µm cell strainers and centrifuged for 5 min at 200 g. Supernatant was  
773 removed and the pellets were resuspended in culture media, SVF cells were plated in a  
774 plate pre coated with collagen I and differentiated as described previously<sup>48</sup>. Cells were  
775 re-fed every 48 hours with 1µM rosiglitazone and 0.5µg/ml insulin. Fully differentiated  
776 adipocytes were stimulated with CL-316,243 (10nM) at day 8 (iBAT).

777 Human HEK 293A cell line (Invitrogen) were grown at 37°C, 5% CO<sub>2</sub> in DMEM  
778 supplemented with 10% FBS and 1% penicillin/streptomycin. All cells in culture were  
779 routinely screened for mycoplasma contamination.

780

### 781 ***In vitro* fertilization**

782 Spermatozoa isolated from cold-treated and control males were used to fertilize oocytes  
783 isolated from superovulated C57BL/6 females. The 4 week old females were

784 superovulated by i.p. administration of 5 IU of equine chorionic gonadotropin (PMSG)  
785 and 5 IU of human chorionic gonadotropin (hCG). Males were sacrificed, the dense  
786 sperm was isolated from cauda epididymis and capacitated in 200ul of Fertiup medium  
787 (Cosmo Bio) for 45 minutes at 37°C, 5% CO<sub>2</sub>. Following sperm capacitation, 2ul of  
788 sperm solution was added to the *IVF* drop consisting of 100 ul HTF medium (Cosmo  
789 Bio) overlaid with embryo tested mineral oil (Sigma). The oviducts were immediately  
790 dissected, and the oocyte clutches released into the IVF drop. The IVF reaction was  
791 carried out for 4 hours at 37°C, 5% CO<sub>2</sub>. Following the IVF, oocytes were washed  
792 several times in M16 medium and the efficiency of fertilization was ascertained by the  
793 appearance of the pronuclei and the 2nd polar body. Fertilized oocytes were surgically  
794 transferred into pseudopregnant CD1 foster females previously mated with genetically  
795 vasectomized Prnm1GFP males<sup>49</sup>.

796

### 797 **Body composition measurement**

798 Body composition was measured with the EchoMRI 130 (Body Composition Analyzer,  
799 Echo Medical Systems). Mice were fasted for 4 hours before measurement.

800

### 801 **Indirect calorimetry**

802 Indirect calorimetry measurements were performed with the Phenomaster (TSE  
803 Systems) according to the manufacturer's guidelines and protocols. Animals were single  
804 caged and acclimated to the metabolic cages for 48 hours before metabolic recording.

805

### 806 **Surface temperature measurement**

807 Surface temperature was recorded with an infrared camera (E60; FLIR; West Malling,  
808 Kent, UK) and analyzed with FLIR-Tools-Software (FLIR; West Malling, Kent, UK)<sup>50</sup>.

809

### 810 **Radio labeled glucose tracing**

811 Tissue radiolabeled glucose uptake was measured as described previously<sup>51</sup>. Animals  
812 were fasted for 4h, then <sup>14</sup>C-2-deoxyglucose at 8 mM, 14.8 MBq/kg body weight was  
813 injected by tail vein. 30 minutes after injection, blood samples were collected, and mice  
814 were sacrificed by cervical dislocation. iBAT, epiWAT, ingWAT, liver, skeletal muscle,  
815 heart and the brain were dissected, weighed and lysed in 10 volumes of 0.5 M NaOH.  
816 Radioactivity was measured by liquid scintillation counting (100 µl of lysate in 3.9 ml of  
817 Emulsifier-Safe, Perkin Elmer).

818

### 819 **Insulin tolerance test (ITT)**

820 Animals were fasted for 4h (Chow diet) and 6h (High fat diet). Blood was collected from  
821 a small incision in the tip of the tail (time 0) and then 15, 30, 60 and 120 min after an i.p.  
822 injection of insulin at 0.6 U/kg (chow) and 0.75 U/kg (HFD) body weight, (Actrapid Penfill,  
823 Novo Nordisk). Blood glucose levels were measured with a blood glucometer (Accu-  
824 Chek Aviva, Roche).

825

### 826 **Behavioral studies**

827 Maternal behavior quantification was carried out as previously reported<sup>52</sup>. 9-week old  
828 virgin female mice were bred with 9-week-old RT or P-CE male mice. All pregnant  
829 females were single caged, and behavior was recorded throughout the pregnancy and

830 nursing by cameras. Maternal nursing behavior was quantified from delivery to postnatal  
831 day 11, based on the video recordings.

832

### 833 **Plasma biochemistry analysis**

834 Mice were fasted for 6h before sacrifice. Blood samples were obtained from cardiac  
835 puncture, and plasma was collected after centrifugation for 15mins at 3000rpm at 4°C.  
836 Cholesterol and triglycerides were measured by enzymatic tests (Roche Diagnostics).  
837 Plasma FGF21 was analyzed using Mouse/Rat FGF-21 ELISA kit (BioVendor). Plasma  
838 insulin levels were measured by Mouse/Rat insulin kit (Meso Scale Discovery). Plasma  
839 samples for measuring fasting/refeeding NEFAs was obtained after 12-h fasting and 4-h  
840 refeeding, by a commercial NEFAs kit (WAKO).

841

### 842 **DNA isolation from sperm and adipose tissue**

843 DNA from sperm and adipose tissue were extracted with the QIAamp DNA Mini Kit  
844 (Qiagen). Sperm samples were isolated from cauda epididymis, resuspended in M2  
845 medium (Sigma) for 45 min at 37°C. Supernatant containing sperm without tissue debris  
846 were collected, pelleted (10,000 g), washed with washing buffer (150 mM NaCl, 10 mM  
847 EDTA pH 8.0), and centrifuged for 10 min at 4000 rpm. The sperm pellet was  
848 resuspended in 300 µl lysis buffer (100 mM Tris·Cl pH 8.0, 10 mM EDTA, 500 mM NaCl,  
849 1% SDS, 2% β-mercaptoethanol).

850

### 851 **DNA pyro-sequencing**

852 500ng DNA (from sperm, adipose tissues or HEK cells) was bisulfite-converted with the  
853 EpiTect Bisulfite Kit (Qiagen) following the manufacturer's protocol. 20 ng of this

854 bisulfite-converted DNA was PCR-amplified with the PyroMark PCR Kit (Qiagen). PCR  
855 amplification and sequencing primers (reverse primers were biotinylated) were designed  
856 using the Pyromark Assay Design v2.0 software (Qiagen). Quality of PCR products were  
857 checked by gel electrophoresis. Pyrosequencing was applied on a PyroMark Q96 ID  
858 using PyroMark Reagents (Qiagen). DNA methylation frequency was quantified with the  
859 PyroMark software (Qiagen). Specific CpG sites are illustrated in **Supplementary Table**  
860 **3**.

861

### 862 ***In vitro* methylation assay**

863 Coding sequence of mouse Adrb3 DNA was ordered from Genscript and cloned into  
864 pCpGfree-mcs vector (Invivogen). HEK293 cells with 80% confluency in 24-well plates  
865 were transfected 1000 ng/well of either methylated or unmethylated constructs with PEI  
866 (Polysciences), at 4:1 ratio to DNA. 24 h after transfection, medium was replaced.  
867 Transfected cells were harvested for analysis at 48 h post transfection.

868

### 869 **Tissue harvest**

870 Animals were euthanized singly in a carbon dioxide atmosphere. Popliteal lymph nodes  
871 were removed from inguinal depots for analyses of gene expression and cellular  
872 separations. Blood was collected by cardiac puncture, and serum was obtained by  
873 centrifuging coagulated blood at 10,000g for 5 min at 4°C.

874

### 875 **Analysis of adipocyte differentiation**

876 Differentiated adipocytes at day 8 were used for differentiation analysis. Briefly, cells in  
877 96 well optical plate were fixed with 5% formaldehyde at 4 °C for 10 min, followed by 3

878 times washing with PBS. Cells were stained with LD540 (100 ng/μl) for lipid droplets<sup>53</sup>  
879 and Hoechst No. 33342 (100 ng/μl). For UCP1 staining, lipids were depleted by 5%  
880 acetic acid in ethanol for 10 min at -20 °C, washed with PBS twice at RT and blocked in  
881 0.05% triton, 5% BSA, PBS. Cells were incubated with UCP1 antibody (1:500) overnight,  
882 washed trice in PBS, incubated with 488 anti-rabbit (1:500) secondary antibody and  
883 DAPI, followed by three washing steps. 29 images per well were taken with an  
884 automated microscope imaging system (Operetta, Perkin Elmer). Images were analyzed  
885 using the Operetta imaging software as described previously<sup>54</sup>.

886

### 887 **Histology and image analysis**

888 Adipose tissues were excised, fixed in fresh 4% paraformaldehyde (Sigma) in PBS  
889 (Gibco; pH 7.4) for 24 h at 4°C and then embedded with paraffin. 4-micron paraffin  
890 sections were subjected to histological staining<sup>55</sup>. Heat induced antigen retrieval was  
891 applied on rehydrated paraffin sections. After blocking with 5% BSA for 1 hour, primary  
892 antibody (1:200 UCP1, Thermo) diluted in 5% BSA was applied to sections overnight at  
893 4 °C. After washing with PBS, a secondary antibody (Signal Stain Boost IHC, Cell  
894 Signaling) was applied and the sections were washed 3 times and were detected using  
895 the DAB method (Cell Signaling). Standard hematoxylin and eosin staining was  
896 performed on rehydrated fat paraffin sections. Slides were dehydrated and covered with  
897 coverslip by resin-based mounting. Analysis of lipid droplet sizes was performed using  
898 ImageJ. For each treatment 21-33 pictures were analyzed. Approximately 18000-58000  
899 lipid droplet objects per mouse were used for the computation of lipid droplet size. Oil  
900 red O staining was applied on liver cyro-sections, as previously described<sup>56</sup>. Liver  
901 samples were excised, fixed with PFA, dehydrated with 30% sucrose and embedded in

902 OCT. 10  $\mu\text{m}$  sections were cut and stained with fresh prepared ORO staining solution.  
903 All images were acquired by Axioscope A.1.

904

### 905 **Fluorescence immunostaining of adipose cryosections**

906 Brown adipose tissues from Ctrl and P-CE animals were excised and fixed in fresh 4%  
907 paraformaldehyde (Sigma-Aldrich) in PBS (Gibco) at pH 7.4 for 2 h at 4 °C, washed four  
908 times in PBS and cryopreserved for 30 h in 30% sucrose in PBS with stirring at 4 °C.  
909 The samples were flash-frozen on dry ice and stored at -80 °C. Brown adipose tissues  
910 were cut at -25 °C on an HM 500 O microtome (Microm) at 20  $\mu\text{m}$  thickness, mounted  
911 on Superfrost plus slides (Medit) and thawed at 4 °C, blocked with 10% donkey serum  
912 in PBS for 1 h, followed by tyrosine hydroxylase antibody overnight incubation 1:200 in  
913 PBS. Sections were washed 3 times in PBS at RT, stained with Alexa 488 anti-rabbit  
914 secondary antibody and 300 nM DAPI for 1 h. Slides were embedded in ProLong®  
915 Diamond Antifade Mountant (Thermo). Fluorescence micrographs were acquired on an  
916 SP5 confocal microscope (Leica). Background was adjusted using samples without  
917 primary antibody.

918

### 919 **Extracellular respiration**

920 Primary brown preadipocytes were counted and plated at a density of 20,000 cells per  
921 well of a seahorse plate and differentiated to confluence. At day 8 post-differentiation  
922 induction, mature brown adipocytes were loaded to XF<sub>24</sub> Extracellular Flux Analyzer  
923 (Seahorse Bioscience), with one injection of CL-316,243 (10 nM).

924

### 925 **RNA extraction, cDNA synthesis, quantitative RT-PCR**



926 Total RNA was extracted from tissues or cells using Trizol reagent (Invitrogen) according  
927 to the manufacturer's instructions. Reverse transcription was performed to generate  
928 cDNA library by using the High Capacity cDNA Reverse transcription kit (Applied  
929 Biosystems), with 1 µg of RNA. Quantitative PCR was performed on a ViiA7 (Applied  
930 Biosystems) and relative mRNA concentrations normalized to the expression of *36B4*  
931 (*Rplp0*) were calculated by the  $\Delta\Delta Ct$  method. Primer sequences are listed in  
932 **Supplementary Table 4.**

933

### 934 **RNA-Sequencing, Mapping and Analysis**

935 RNA from brown adipose tissue were quality checked by tape station (GE). All samples  
936 had a RIN value of greater than 8. The ribosomal RNA was depleted, and purified RNA  
937 was used for the preparation of libraries using the TruSeq RNA sample preparation kit  
938 (Illumina) and sequenced on a HiSeq 4000 HT. RNA-seq sequences were trimmed  
939 using Trim Galore (v0.4.4,  
940 [http://www.bioinformatics.babraham.ac.uk/projects/trim\\_galore/](http://www.bioinformatics.babraham.ac.uk/projects/trim_galore/)) and mapped to the  
941 mouse GRCm38 genome assemblies using hisat2 (v2.1.0). Transcripts were defined  
942 using the Ensemble annotations over protein-coding mRNAs. Differential expression  
943 analysis of mapped RNA-seq data was performed using DESeq2<sup>57</sup> and EdgeR.  
944 Significantly different transcripts were called with significance below 0.05 after  
945 Benjamini and Hochberg correction and minimum mean differential expression of 2-fold.  
946 Further analysis were performed using SeqMonk software  
947 ([www.bioinformatics.babraham.ac.uk/projects/seqmonk/](http://www.bioinformatics.babraham.ac.uk/projects/seqmonk/)). Quantitation of RPM values  
948 was performed using the SeqMonk RNA-Seq pipeline quantitation on merged transcripts  
949 counting reads over exons correcting for DNA contamination and log2 transformed

950 assuming an opposing strand specific library transformed by percentile normalization  
951 using “Add” to the 75.0 percentile. Gene ontology (GO) analysis were performed using  
952 the g:profiler software (<http://biit.cs.ut.ee/gprofiler/>). Expressed genes were defined  
953 where at least 1 of all 4 groups (CTRL-3CE, CTRL-RT, P-CE-3CE, P-CE-RT) had a  
954 log<sub>2</sub>(RPM) value above zero. Transcriptional similarities between the different samples  
955 were computed on all expressed genes using hierarchical clustering (R hclust package)  
956 with Euclidian distances and by applying the Ward distance function and plotted as a  
957 dendrogram. PCA was performed using the R prcomp package with default parameters.

958

### 959 **Whole-Genome Bisulfite Sequencing**

960 Mapping and Analysis Genomic sperm DNA was isolated as described and used for  
961 whole-genome bisulfite (WGBS) libraries<sup>58</sup>. Briefly, WGBS libraries were prepared by  
962 sonicating 500ng genomic DNA using a Covaris Sonicator into 300-400bp long  
963 fragments, followed by end-repair, A-tailing and methylated adapter (Illumina) ligation  
964 using NEB-Next reagents. Libraries were bisulfite treated using EZ DNA Methylation-  
965 Direct Kit (Zymo), followed by library amplification with indexed primers using KAPA HiFi  
966 Uracil+ HotStart DNA Polymerase (Roche). All amplified libraries were purified using  
967 AMPure XP beads (Agencourt) and assessed for quality and quantity using High-  
968 Sensitivity DNA chips (Agilent Bioanalyzer). High-throughput sequencing of all libraries  
969 was carried out with a 125 bp paired-end protocol on a HiSeq 2000 instrument  
970 (Illumina). Raw sequence reads from WGBS libraries were trimmed to remove poor  
971 quality reads and adapter contamination, using Trim Galore (v0.4.4,  
972 [http://www.bioinformatics.babraham.ac.uk/projects/trim\\_galore/](http://www.bioinformatics.babraham.ac.uk/projects/trim_galore/)). The remaining  
973 sequences were mapped using Bismark (v0.18.0)<sup>59</sup> with default parameters to the

974 mouse reference genome GRCm38 in paired-end mode. Reads were deduplicated and  
975 CpG methylation calls were extracted from the deduplicated mapping output using the  
976 Bismark methylation extractor (v0.18.0) in paired-end mode. CpG methylation calls were  
977 analyzed using R and SeqMonk software  
978 ([www.bioinformatics.babraham.ac.uk/projects/seqmonk/](http://www.bioinformatics.babraham.ac.uk/projects/seqmonk/)). The genome was divided into  
979 consecutive probes overlapping 50 CpGs each and percentage methylation was  
980 calculated using the bisulfite feature methylation pipeline in SeqMonk. Global CpG  
981 methylation levels were illustrated using box whisker plots and promoter methylation  
982 similarities between the samples were assessed using hierarchical clustering (R hclust  
983 with Pearson distances and Ward distance function) and PCA (R prcomp package with  
984 default parameters). CpG island (CGI) methylation levels were calculated using the  
985 SeqMonk bisulfite feature methylation pipeline and averaged over all CpG islands for  
986 illustrations. DMRs were calculated using the SeqMonk binomial filter on probes (50  
987 CpG probes or CGIs) with significance below 0.05 after multiple testing correction and a  
988 minimum difference of 10%. Gene ontology analysis were performed using the g:profiler  
989 software (<http://biit.cs.ut.ee/gprofiler/>) with genes which either overlapped with DMRs or  
990 where up to 2kb downstream of the DMR. DMRs were divided into hypermethylated or  
991 hypomethylated in the paternal cold exposure vs control samples. The expression levels  
992 in brown adipose tissue samples of transcripts overlapping with DMRs (logistic  
993 regression filter; see above) either hypermethylated or hypomethylated in the P-CE vs Ctrl  
994 samples was computed using the log2 RPM gene expression levels in Ctrl brown  
995 adipose tissue samples.

996

997 **Western Blot**

998 Protein samples were isolated from adipose tissue with RIPA buffer (50 mM Tris-HCl pH  
999 (7.5), 150 mM NaCl, 1mM EDTA, 1% Triton X-100, 0.1% SDS, 10% glycerol)  
1000 supplemented with protease inhibitor cocktail (Roche) and Halt Phosphatase Inhibitor  
1001 (Thermo). Homogenized protein lysates were obtained by rotating at 4 °C for 30 min,  
1002 followed by centrifugation at 14,000 rpm for 30 min. Protein amounts were quantified  
1003 using the DC Protein Assay (Bio-Rad). For immunoblotting, protein samples were  
1004 separated by SDS-PAGE on 12% polyacrylamide gels and transferred onto  
1005 nitrocellulose membrane. Membranes were probed using the indicated antibodies and  
1006 chemiluminescent signals was detected by a LAS 4000 mini Image Quant system (GE  
1007 Healthcare). Band intensity was quantified using ImageJ. Uncropped full scan blots are  
1008 shown in **Supplemental Fig. 9-11**.

1009

#### 1010 ***In vivo* microdialysis from iBAT**

1011 For measuring the release of norepinephrine from iBAT a microdialysis probe was  
1012 implanted subcutaneously on the back of the animal one hour before the start of the  
1013 experiment (CMA 20 custom made, 3mm membrane, cutoff 20,000 kDa, CMA,  
1014 Sweden). The microdialysis probe was connected to a pump that flushes artificial  
1015 cerebrospinal fluid (147 mM Na<sup>+</sup>, 2.4 mM Ca<sup>2+</sup>, 4 mM K<sup>+</sup>, 155.6 mM Cl<sup>-</sup>, pH 6.0) through  
1016 the probe at a follow rate of 1.5 ul/min. The tube was connected to the animal via a  
1017 movable arm to allow free movement. After stabilization, samples were collected at 30-  
1018 min intervals through a refrigerated fraction sampler (MAB 85, Microbiotech AB,  
1019 Sweden). After baseline samples at RT were collected, temperature was reduced to 8°C  
1020 for a period of 3-hours.

1021

## 1022 **HPLC norepinephrine assessment**

1023 Dialysate samples from BAT were immediately frozen and stored at  $-80^{\circ}\text{C}$  until  
1024 injection onto the high-performance liquid chromatography (HPLC; Ultimate 3000,  
1025 Thermo Scientific, US) system. Norepinephrine levels were detected and analyzed using  
1026 an electrochemical detector (ECD-3000RS, Thermo Scientific, US) with a coulometric  
1027 cell (6011RS, Thermo Scientific, US). The samples were injected via a refrigerated  
1028 autoinjector (Thermo Fisher, CA, USA) equipped with a  $100\ \mu\text{l}$  injection loop. Samples  
1029 were separated on a reversed-phase column ( $4.6\times 80\text{mm}$ ,  $3\ \mu\text{m}$  Thermo Fisher, US). We  
1030 used a HPLC pump (ISO-3100BM, Thermo Fisher, CA, USA) and a mobile phase of  
1031 ammonium acetate, EDTA, 15% methanol, 5% acetonitrile adjusted to pH of 6.0, at a  
1032 flow rate of  $0.3\ \text{ml/L}$  at  $32^{\circ}\text{C}$ . A chromatography workstation (Chromeleon, Thermo  
1033 Fisher Scientific, Switzerland) was used for data acquisition and calculation.

1034

## 1035 **Statistical analyses**

1036 For *in vivo* studies, age-matched male mice were used for all experiments. Sample sizes  
1037 were determined on the basis of previous experiments using similar methodologies. P-  
1038 CE and Ctrl fathers always were derived from same litters and were handled in the same  
1039 manner. One to two offspring were used from each litter for all experiments. The number  
1040 of litters analyzed for all experiments are indicated in the corresponding figure legends.  
1041 If more than one mouse from one litter was used the mice were analyzed as technical  
1042 replicates. In total more than 60 litters per group were analyzed for P-CE and Ctrl mice,  
1043 respectively. Mice were randomly assigned to treatment groups. All animals were  
1044 included for statistical analyses, and the investigators were not blinded. RNA and DNA  
1045 methylation sequencing analyses were blinded to experimental conditions. Results are

1046 reported as mean  $\pm$  SEM. Two-tailed unpaired Student's *t*-test was applied on  
1047 comparison. ANOVA was applied on comparisons which involve multiple groups.  
1048 Statistical differences were indicated as \* for  $P < 0.05$ , \*\* for  $P < 0.01$  and \*\*\* for  $P < 0.001$ .

1049

#### 1050 **DATA AND SOFTWARE AVAILABILITY**

1051 The accession number for the WGBS next-generation-sequencing data reported in this  
1052 study is GEO: GSE100231. RNA sequencing data was uploaded to European  
1053 Nucleotide Archive (ENA) with accession number PRJEB15274.

1054 **References for methods**

- 1055 46. Becker, A.S., Nagel, H.W., Wolfrum, C. & Burger, I.A. Anatomical Grading for Metabolic  
1056 Activity of Brown Adipose Tissue. *PLoS One* **11**, e0149458 (2016).
- 1057 47. Ho, D.E., Imai, K., King, G. & Stuart, E.A. Matching as nonparametric preprocessing for  
1058 reducing model dependence in parametric causal inference. *Polit Anal* **15**, 199-236  
1059 (2007).
- 1060 48. Kazak, L., *et al.* A creatine-driven substrate cycle enhances energy expenditure and  
1061 thermogenesis in beige fat. *Cell* **163**, 643-655 (2015).
- 1062 49. Haueter, S., *et al.* Genetic vasectomy-overexpression of Prm1-EGFP fusion protein in  
1063 elongating spermatids causes dominant male sterility in mice. *Genesis* **48**, 151-160  
1064 (2010).
- 1065 50. Whittle, A.J., *et al.* BMP8B increases brown adipose tissue thermogenesis through both  
1066 central and peripheral actions. *Cell* **149**, 871-885 (2012).
- 1067 51. Abreu-Vieira, G., *et al.* Cidea improves the metabolic profile through expansion of  
1068 adipose tissue. *Nature communications* **6**, 7433 (2015).
- 1069 52. Pryce, C.R., Bettschen, D., Nanz-Bahr, N.I. & Feldon, J. Comparison of the effects of  
1070 early handling and early deprivation on conditioned stimulus, context, and spatial  
1071 learning and memory in adult rats. *Behav Neurosci* **117**, 883-893 (2003).
- 1072 53. Spandl, J., White, D.J., Peychl, J. & Thiele, C. Live cell multicolor imaging of lipid  
1073 droplets with a new dye, LD540. *Traffic* **10**, 1579-1584 (2009).
- 1074 54. Meissburger, B., *et al.* Adipogenesis and insulin sensitivity in obesity are regulated by  
1075 retinoid-related orphan receptor gamma. *EMBO Mol Med* **3**, 637-651 (2011).
- 1076 55. Sanchez-Gurmaches, J. & Guertin, D.A. Adipocytes arise from multiple lineages that are  
1077 heterogeneously and dynamically distributed. *Nature communications* **5**, 4099 (2014).
- 1078 56. Mehlem, A., Hagberg, C.E., Muhl, L., Eriksson, U. & Falkevall, A. Imaging of neutral  
1079 lipids by oil red O for analyzing the metabolic status in health and disease. *Nature*  
1080 *protocols* **8**, 1149-1154 (2013).
- 1081 57. Love, M.I., Huber, W. & Anders, S. Moderated estimation of fold change and dispersion  
1082 for RNA-seq data with DESeq2. *Genome Biol* **15**, 550 (2014).
- 1083 58. von Meyenn, F., *et al.* Comparative Principles of DNA Methylation Reprogramming  
1084 during Human and Mouse In Vitro Primordial Germ Cell Specification. *Dev Cell* **39**, 104-  
1085 115 (2016).
- 1086 59. Krueger, F. & Andrews, S.R. Bismark: a flexible aligner and methylation caller for  
1087 Bisulfite-Seq applications. *Bioinformatics* **27**, 1571-1572 (2011).

Figure 1

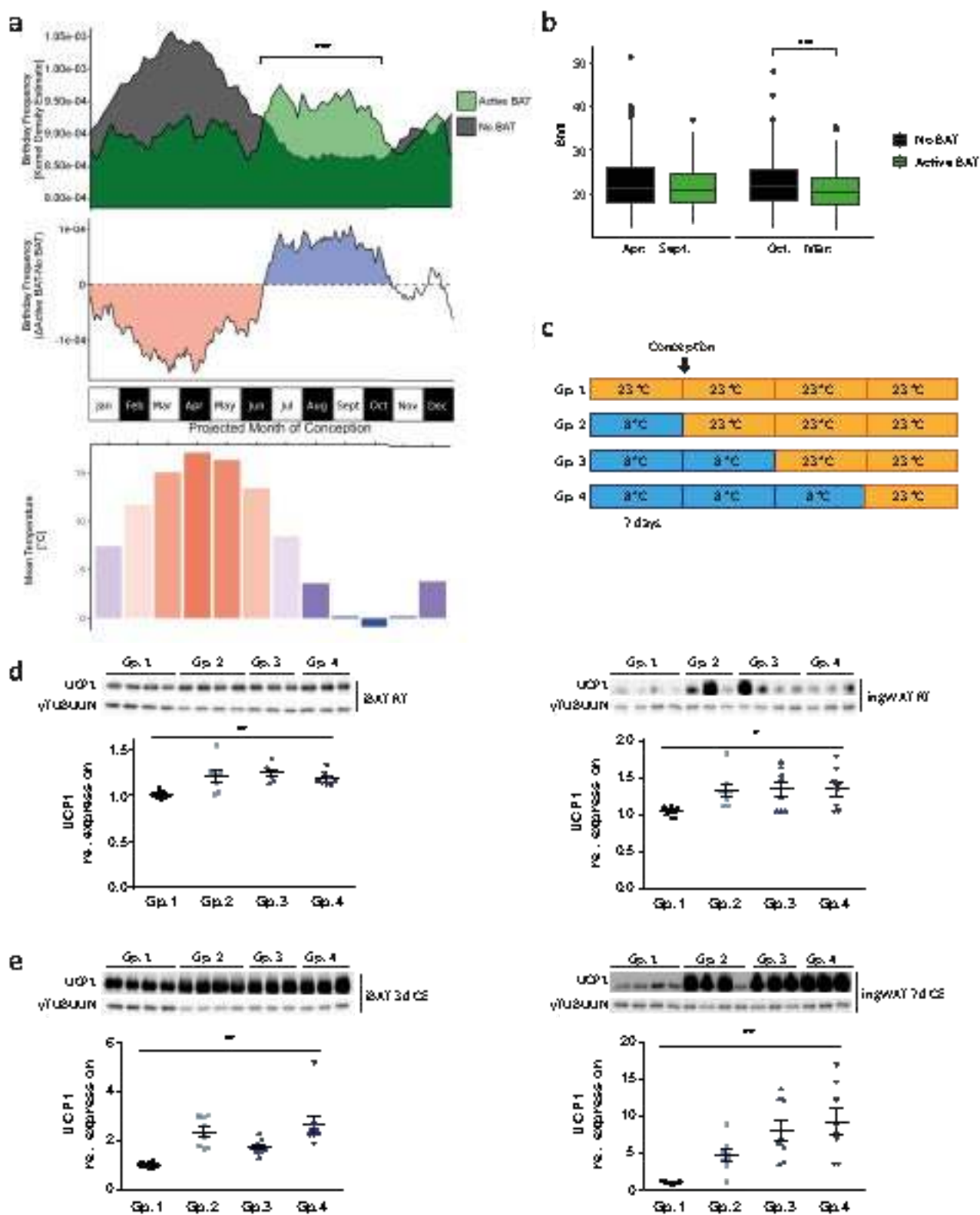




Figure 2

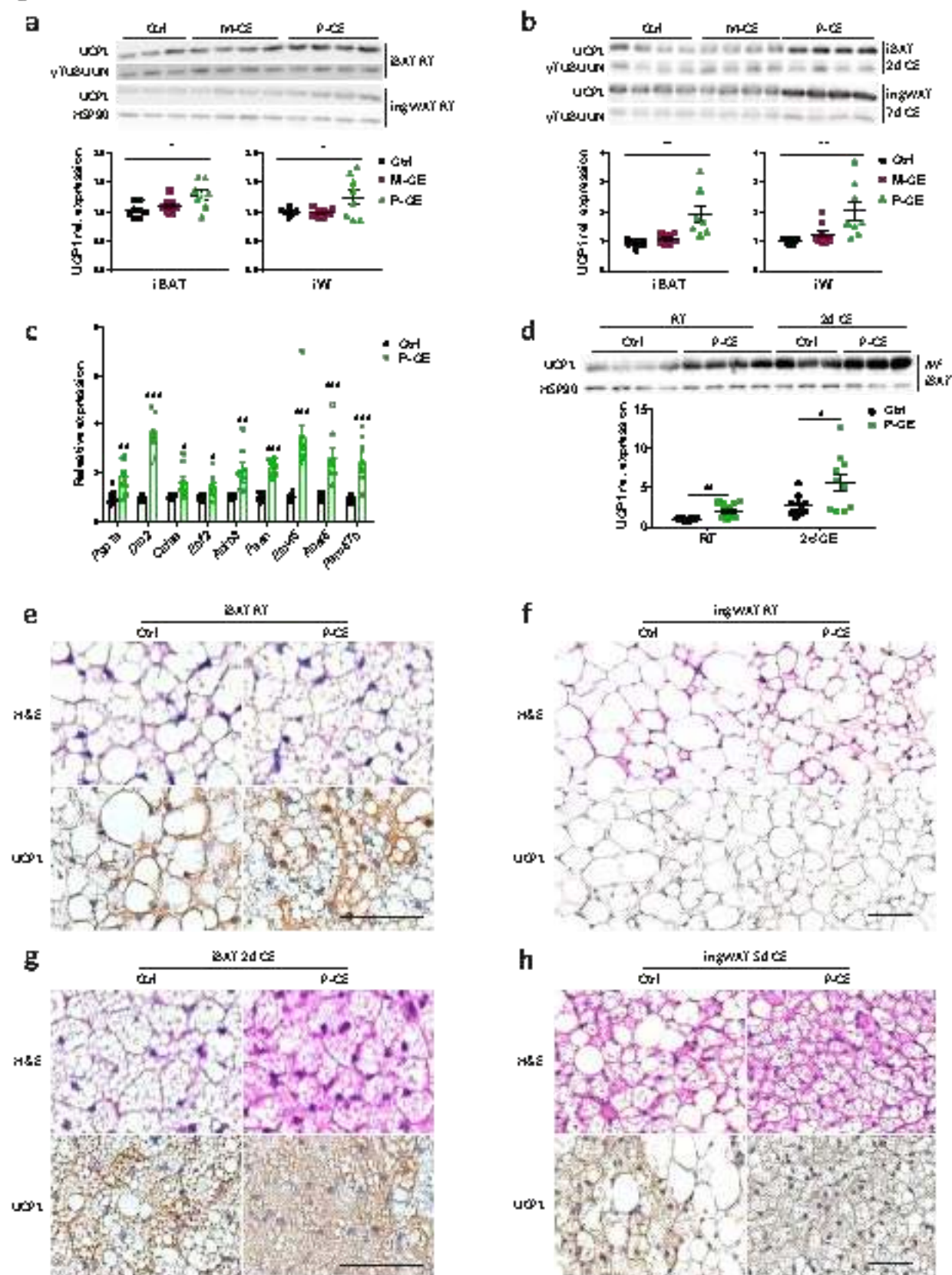


Figure 3

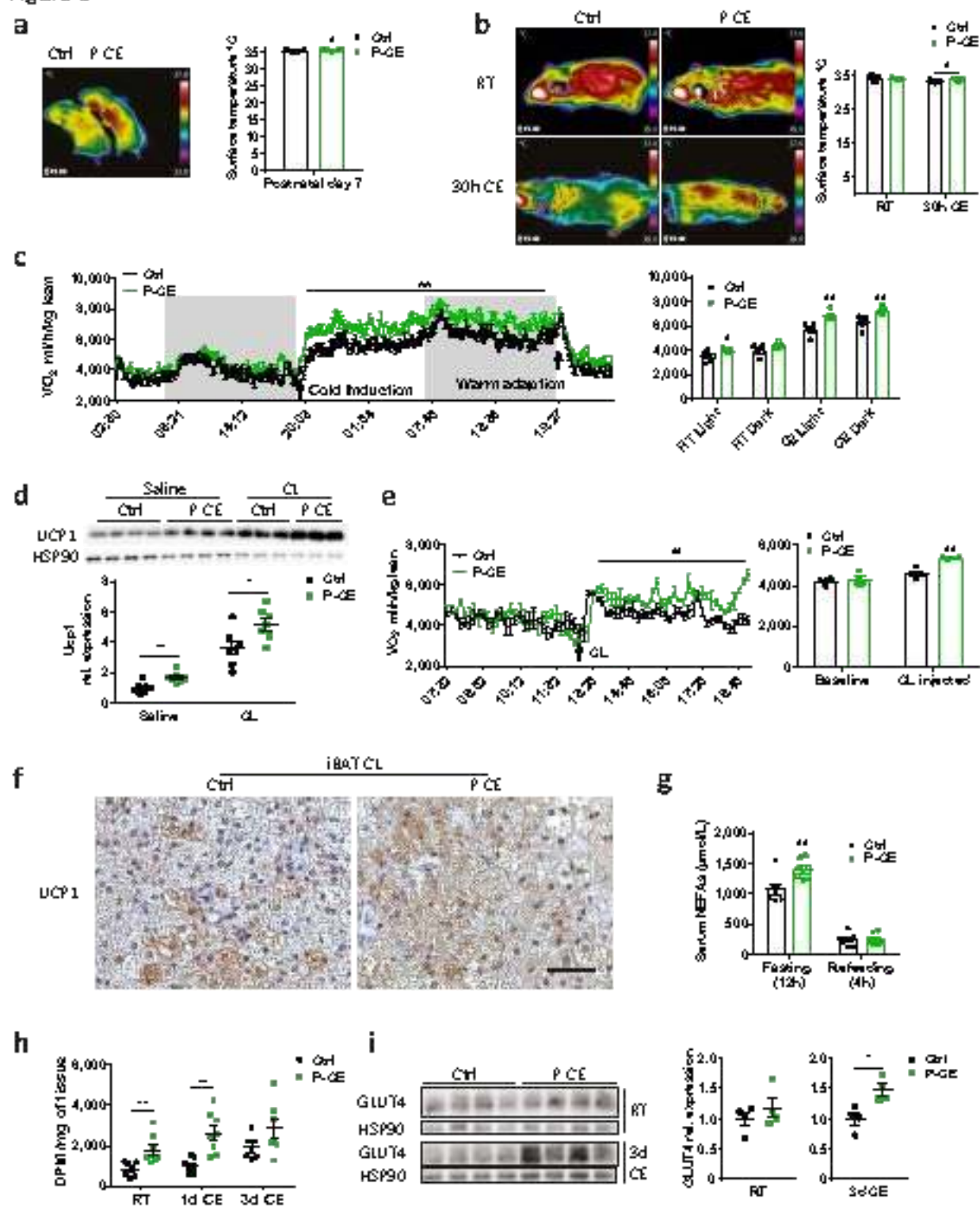


Figure 4

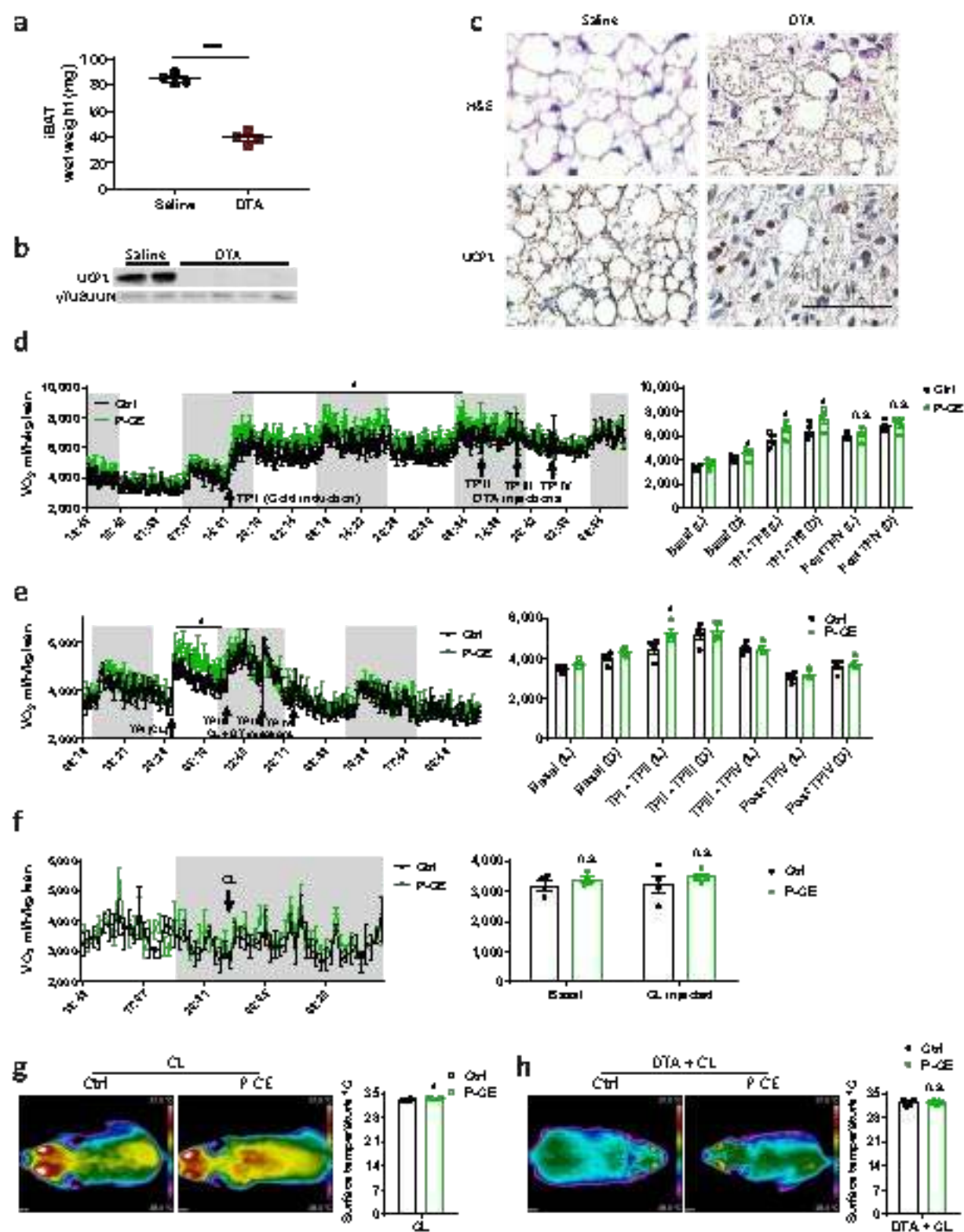
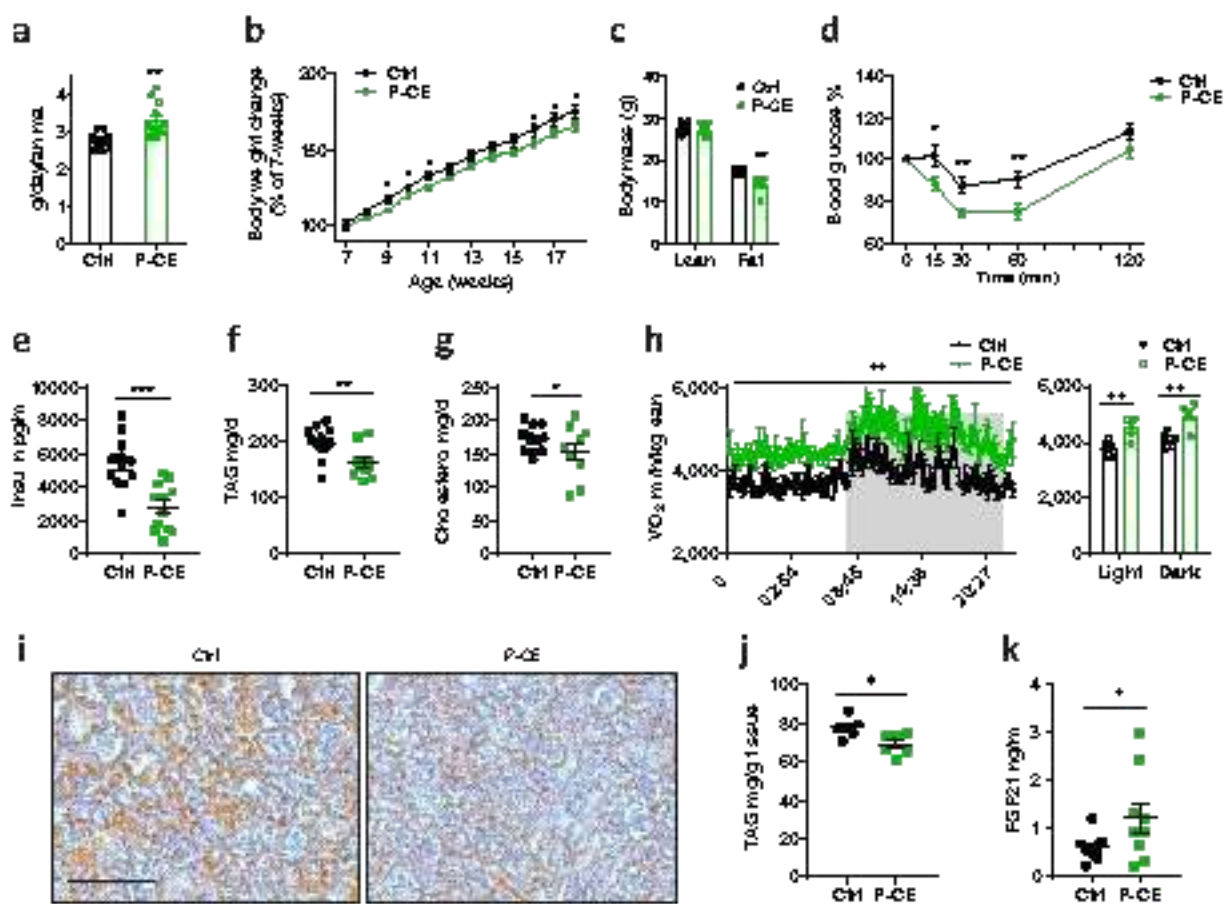


Figure 5





**Figure 6**

